Schweizerische Eidgenossenschaft
Confédération suisse
Confederazione Svizzera
Confederaziun svizra

Department of the Environment,
Transport, Energy and Communication DETEC

Swiss Federal Office of Energy SFOE
Energy Research

Final report dated March 31, 2021

PMU-based adaptive protections for active distribution grids

SynchroFAP (Synchrophasors For Adaptive Protection)

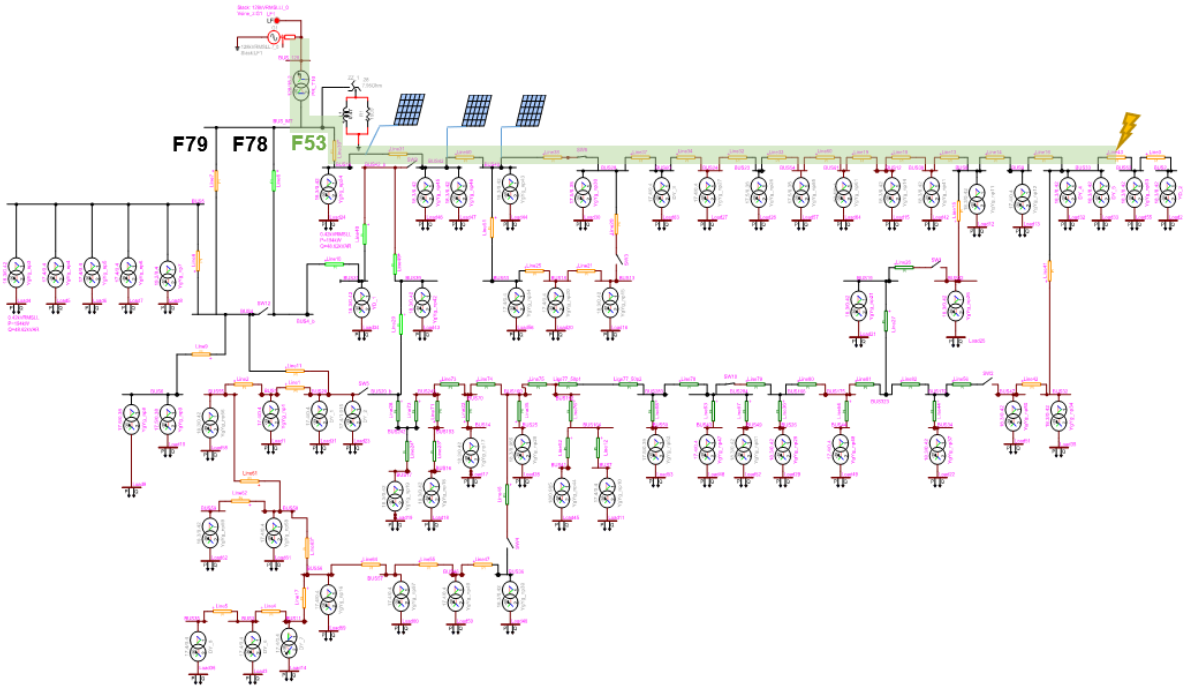

Date: March 31, 2021

Location: Bern

Publisher:
Swiss Federal Office of Energy SFOE
Energy Research and Cleantech
CH-3003 Bern
www.bfe.admin.ch

Subsidy recipients:
HES-SO // Valais – Wallis
Rte du Rawil, 47, CH-1950 Sion
www.hevs.ch

Zaphiro Technologies SA
Chemin de la Raye 13, CH-1024 Ecublens
www.zaphiro.ch

DESL-EPFL
ELL 136 (Bâtiment ELL), Station 11, CH-1015 Lausanne

Cottens & Badoux Energie Services SA (CESSA)
Chemin de la Outre 2, CH-1429 Giez

Helinks LLC
Chollerstrasse 3, CH-6300 Zug

Authors:
Davide, Pavanello, HES-SO // Valais – Wallis, davide.pavanello@hevs.ch
Lorenzo, Zanni, Zaphiro Technologies SA, lorenzo.zanni@zaphiro.ch
Marco, Pignati, Zaphiro Technologies SA, marco.pignati@zaphiro.ch

SFOE project coordinator:
Michael, Moser, michael.moser@bfe.admin.ch

SFOE contract number: SI/501724-01

The authors bear the entire responsibility for the content of this report and for the conclusions drawn therefrom.

Zusammenfassung

Wenn man die Architektur von Stromversorgungssystemen betrachtet, ist die Verteilungsebene diejenige, die in letzter Zeit aufgrund der verteilten Erzeugung aus erneuerbaren Energien eine ständige Aufrüstung erfährt. Die Nachfrage nach einer verbesserten Beobachtbarkeit von Mittelspannungsnetzen wächst weiter und der Einsatz von Phasor Measurement Units (PMUs) wird in Zukunft bei den Verteilnetzbetreibern sicherlich immer beliebter werden. Aus diesem Grund müssen neue Techniken, wie z.B. adaptive Schemata, entwickelt werden, um die Vorteile einer solchen erweiterten Sichtbarkeit des Netzzustandes für Schutzzwecke nutzen zu können. Das BFE unterstützt die Forschung im Bereich des Netzschutzes in der Schweiz. Insbesondere das Projekt SynchroFAP ermöglicht es akademischen Forschern und Experten aus der Praxis, ihre Anstrengungen zu bündeln und gleichzeitig neue Grenzen der Schutzsysteme für Verteilnetze zu erforschen.

Résumé

En ce qui concerne l'architecture des systèmes électriques, la couche de distribution est celle qui, ces derniers temps, fait l'objet d'une mise à niveau constante en raison de la production décentralisée provenant des énergies renouvelables. La demande d'une meilleure observabilité des réseaux de moyenne tension continue de croître et l'adoption d'unités de mesure de Phasor Measurement Units (PMU) deviendra certainement plus populaire parmi les opérateurs de systèmes de distribution à l'avenir. C'est pourquoi, afin de profiter de cette visibilité accrue de l'état du réseau à des fins de protection, de nouvelles techniques comme les protections adaptatifs doivent être développées. L'OFEN soutient la recherche sur la protection des réseaux électriques en Suisse et le projet SynchroFAP, en particulier, permet aux chercheurs universitaires et aux experts du domaine pratique de joindre leurs efforts tout en explorant les nouvelles frontières des systèmes de protection des réseaux de distribution.

Summary

Considering power systems architecture, distribution layer is the one which lately experiences constant upgrading because of dispersed generation coming from renewables. Demand for improved observability of medium-voltage grids continues growing and the adoption of Phasor Measurement Units (PMUs) will certainly become more popular among distribution system operators in the future. For this reason, in order to take advantage of such augmented visibility of grid state for protection purposes, new techniques like adaptive schemes need to be developed. The SFOE has been supporting power system protection research in Switzerland and the project SynchroFAP, in particular, allows academic researchers and experts from the practical field to join their efforts while exploring new frontiers of protection systems for distribution networks.

Main findings

- We found out that increasing amount of DGs is threatening distribution grid reliability when a fault occurs (e.g., blinding effect). Therefore, DGs need to be included in the short-circuit analysis.
- We developed an innovative optimization method based on PMU measurements to identify ZIP model of clusters of loads/generators. They accurate represent loads/generators behaviour in the short-circuit analysis. In this way, we can automatically adapt relay settings to properly protect the grid.
- We demonstrated the developed method with a real-time hardware-in-the-loop simulation including a real relay and standard-compliant communication protocols.

Contents

Abbreviations

DG	Distributed Generation
DSO	Distribution System Operator
EMTP-RV	ElectroMagnetic Transient Program – Revised Version
HV	High Voltage
LV	Low Voltage
MV	Medium Voltage
PMUs	Phasor Measurement Units
PV	Photovoltaic
OC	Overcurrent
SC	Short-Circuit
SFOE	Swiss Federal Office of Energy
SIG	Services Industriels de Genève
WPx	xth Work Package
ZIP	Z for Impedance, I for Current, P for Power

1 Introduction

1.1 Background information and current situation

Traditionally, energy distribution has always been following the same paradigm: large power plants to feed loads through transmission and distribution networks, essentially by mono-directional power flows. Today, smaller decentralized production units (mostly photovoltaic panels in Switzerland) are being massively installed at medium voltage (MV) and low voltage (LV) levels, as a major response to national decarbonization strategies. As an example, the objective of the Canton of Geneva is to reach 350 MW of installed PV nominal power by 2030 (with respect to around 50 MW today).

Most of the power systems in operation were conceived several decades ago according to the traditional architecture described above, for which it is well known today that a strong amount of distributed generation (DG) would not come without issues. Most frequently, the criteria adopted to assess grid robustness against DG penetration are the capability of the voltage level to remain within the boundaries and the lines not to approach overloading, which often guarantee acceptable power quality levels. Less frequently this assessment involves protection aspects, at least on a first stage of reflection.

It is well known from the literature that conventional protection schemes might fail in presence of important shares of DG due to situations referred to as blinding and sympathetic tripping (which will be explained in Section 3.3.1). Such threats to the reliability of the protection scheme in use depend on the actual output power of the DG, excluding the possibility of adapting the protection settings statically.

1.2 Purpose of the project

The project aims at providing a flexible solution to adapt the reaction of the protection scheme to any grid condition, thanks to the augmented grid observability that would be provided by phasor measurement units (PMUs). Knowing the status of the grid at any time would allow modifying the threshold of the protection functions accordingly, in particular to the actual output power of DG. The purpose of this project is to demonstrate the feasibility of this approach, both theoretical and technical, thus establishing a first milestone towards a future ground-proof validation on the real grid.

1.3 Objectives

A first goal of the SynchroFAP project is to show the vulnerability of a conventional protection scheme for distribution grid against a large amount of DG.

Secondly, the project aims at developing a new modeling procedure for the behavior of load/generation clusters, based on the concept of ZIP parameters, to be efficiently used in short-circuit analysis.

The project has then the objective of designing an adaptive protection scheme capable of responding correctly to a fault in presence of large amounts of DG.

Finally, the project aims to demonstrate the practical feasibility of the proposed approach, by means of a technical demonstration performed using commercial protection relays.

2 Procedures and methodology

2.1 Modeling of the grid topology in EMTP-RV

Significant portions of the MV network of SIG have been modelled in EMTP-RV. Intense exchange of information between HES-SO Valais // Wallis and the Distribution System Operator (DSO) has been necessary to reproduce the grid topology with satisfactory level of completeness. The grid model, originally developed in DIgSILENT PowerFactory by SIG, was rebuilt in EMTP-RV to perform time domain simulations, more suitable for short-circuit studies.

The MV grid selected for this project is neutral-compensated and operated at 18 kV. Neutral-compensated means that adjustable arc-suppression coils (Petersen coils) are installed between the neutral point of the transformer and the ground at the medium-voltage side of each primary substation. In case of single-phase-to-ground faults, this earthing scheme, often adopted for MV grids, results in relatively low values of fault currents. If this has the considerable advantage of maintaining power supply to the customers during phase-to-ground faults, the inevitable drawback is represented by more challenging fault detection.

Each of the selected grid portions is connected to one primary substation at a time, operated in open loop, with the possibility of being reconfigured if needed. Secondary substations are modelled as well, and the amount of absorbed power was estimated as about one fourth of the nominal MV/LV transformer rating.

Figure 1 shows the resulting EMTP-RV model of one of the selected portions of the considered MV grid. For sake of simplicity, only simulation results obtained using the grid topology shown in Figure 1 are presented in the main part of this report to illustrate the mechanisms involved with DG that might lead to malfunctioning of the protection system. The same considerations apply to the remaining portions of the distribution grid that have been selected within the project and the detailed results of the parametric analysis performed are available in the Appendices.

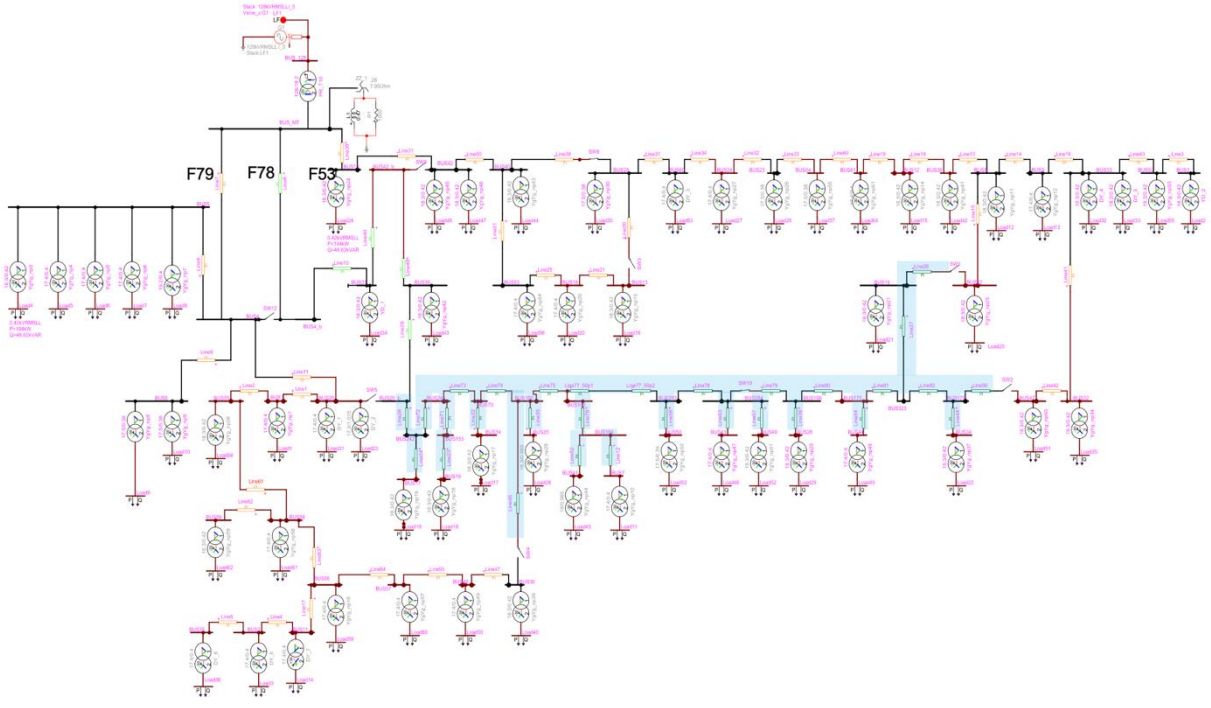

Figure 1 - Example of a selected portion of the MV grid of SIG modeled in EMTP-RV (the lines highlighted in blue are overhead)

2.2 Modeling of load and generation by means of ZIP models

2.2.1 Load models for distribution systems

A number of different complex loads are generally connected to MV and LV distribution networks. The exact decomposition of those loads and their specific electrical characteristics are usually not known by the DSO. An accurate modeling of each device is thus practically impossible. Therefore, loads connected to a single node are generally represented by an aggregated load model in power system studies. An aggregated load will thus represent a number of different devices fed by a MV or LV node together with the interconnecting network components. DG and voltage transformers may be included as well.

As presented in [1], aggregated load models are subdivided into static and dynamic models, depending on whether they are time-independent or not. The most frequently used static load models are the exponential and polynomial/ZIP load models described here below. However, for our studies we will adopt a time-dependent version of the ZIP model, as explained in Section 2.2.4.

Exponential load model: the consumed active and reactive powers depend exponentially on the RMS value of the node voltage and on the relative change of the network frequency, as shown in Eq. (1).

$$P(V,f) = P_n \left(\frac{V}{V_n}\right)^{k_{pu}} \left(1 + k_{pf}\Delta f\right)$$
$$Q(V,f) = Q_n \left(\frac{V}{V_n}\right)^{k_{qu}} \left(1 + k_{qf}\Delta f\right) \quad (1)$$

where $\Delta f = \frac{f - f_n}{f_n}$

The symbols P_n and Q_n denote respectively the nominal consumed active and reactive powers, V_n the RMS value of the nominal node voltage and f_n the nominal power frequency. The symbols k_{pu} and k_{qu} are, respectively, the real and reactive power sensitivities to the node input voltage. If they are set to 0, 1 or 2, the load behaves as a constant power, constant current or constant impedance load, respectively.

Polynomial load model: by removing the dependency on f, the functions P(V) and Q(V) can be developed in Taylor series. By truncating this expansion to the 2nd order we obtain the so-called ZIP equivalent shown in Eq. (2).

$$P(V) = P_n \left[Z_p \left(\frac{V}{V_n}\right)^2 + I_p \left(\frac{V}{V_n}\right)^2 + S_p\right]$$
$$Q(V) = Q_n \left[Z_q \left(\frac{V}{V_n}\right)^2 + I_q \left(\frac{V}{V_n}\right)^2 + S_q\right] \quad (2)$$

The abbreviation ”ZIP” is used since the model consists of three parallel branches, namely, a constant impedance (Z), a constant current generator (I) and a constant power generator (P) with respective participation coefficients ($Z_{p/q}$, $I_{p/q}$, $S_{p/q}$).

There also exist specific static load representations for induction machines and power electronic devices. These models are device specific, which allows to represent the load more accurately. However, they require more knowledge from DSO side about the devices connected to the grid.

2.2.2 Load and generator models commonly used in short-circuit analysis

Short-circuit analyses are a very important tool used by DSOs to evaluate the security of the electrical network and to verify the correct tuning of the protection devices. Short-circuit current levels are calculated at various points of the grid and multiple types of faults are simulated. The settings of protection relays can then be tuned in order to disconnect the smallest area of the grid affected by the fault in the shortest time possible.

Traditionally, short-circuit analyses are performed modeling the passive loads as constant impedance loads, or even setting the current contributions from passive loads to 0 assuming that they are much smaller than the fault currents. Short-circuit current contributions from large induction motors can be calculated knowing the characteristics of the specific machines [2]. Almost all the generators in distribution systems are interfaced to the grid with power converters so that their short-circuit current contribution is limited to the nominal current of the inverter to protect the inverter itself. Additionally, the contribution of DG units to the short-circuit current has been always neglected because their protection devices are usually set to disconnect the generators from the grid when a fault occurs.

However, the amount of distributed generators present in distribution grids has increased during the past years and Fault Ride Through (FTR) capabilities are more and more required [3]. DGs will thus contribute to the short-circuit currents and have to be included in the short-circuit analyses. Otherwise, the estimation of the currents might be affected by large errors and phenomena like *blinding* and *sympathetic tripping* (described in Section 2.4.1) will not be recognized.

In [4], the authors present a short-circuit analysis procedure suitable for distribution systems with a high penetration of DG. They include models of synchronous and induction machines directly connected to the grid, as well as doubly-fed induction generators and inverter-based distributed generators. They can accurately compute short-circuit currents of grids with both passive and active loads. The drawback of this method is however that detailed information is needed about the specific distributed generators to set the parameters of the used models.

Our approach presented in the next section only relies on measurement data at grid nodes and some basic information about the load types.

2.2.3 Static ZIP model

Since we focus on the modeling of the behavior of loads and generators during short-circuits which are characterized by significant voltage variations, we are interested in the voltage dependency of the model rather than the frequency. Therefore, we have chosen to use the ZIP model to represent aggregated loads and generations during steady-state and faulty conditions. Regarding the voltage dependency, the ZIP model also has more degrees of freedom than the exponential load model.

The behaviour of the ZIP model with respect to voltage variations is defined by the linear combination of constant power and current sources and an impedance connected in parallel (see Eq (2)). The equivalent electrical representation is shown in Figure 2.

- The constant power source (S_c) always draws the complex power $P_nS_p + jQ_nS_q$.
- The constant current source (I_c) draws a current to absorb the complex power $P_nI_p + jQ_nI_q$ at nominal voltage. The absorbed apparent power of this branch thus varies linearly with the input voltage (V).
- The parallel RLC circuit forms the equivalent impedance Z. The values are set such that the apparent power $P_nZ_p + jQ_nZ_q$ is absorbed at nominal voltage. The Z-branch draws a total power varying quadratically with the input voltage.

To represent a 3-phase aggregation of loads and generations connected to a specific node, we use 3 equivalent ZIP circuits connected using the Star configuration. Depending on the treatment of the neutral, the Star point may be grounded or not.

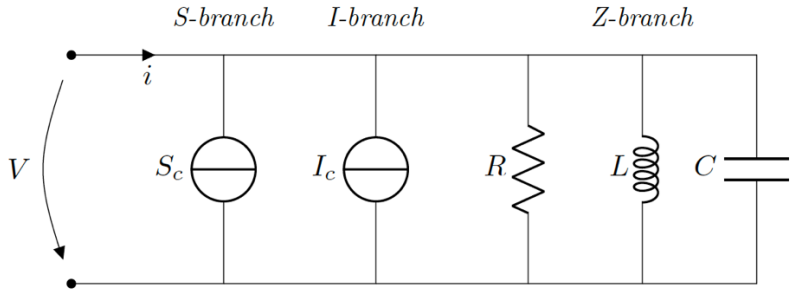

Figure 2 – ZIP equivalent electrical circuit.

2.2.4 Time-dependent ZIP model

The load/generator model needs to be accurate during steady-state and also faulty conditions. Rather than using the static ZIP model described above, we use a time-dependent ZIP model which takes into account the dynamic reaction of the load/generator to voltage changes and we investigate its validity for different network conditions.

The three ZIP branches adapt their current outputs based on the input voltage. The constant current source adapts its phase to draw a constant apparent power for a given RMS value of the node voltage. The constant power source adapts both its phase and current amplitude to always draw the same apparent power.

To simulate the dynamic behaviour of aggregated loads, a node input voltage estimation is added to the classic ZIP model. The voltage frequency and phase angles are estimated using a Phase Locked Loop (PLL), where PI-controllers are used to control the convergence. This gives us two dynamic parameters for the ZIP model, the proportional gain K_p and integral gain K_i, which need to be identified. The static ZIP parameters are those describing the equivalent electrical circuit in Figure 2. In addition, the upper limit $\hat{I}^S_{max}$ of the constant power source has to be identified, allowing to model a saturation which may be present in the true device.

We also add an estimation of the RMS value of the node voltage based on the measured voltage waveform and control the I- and S-branches to generate currents only for voltages ≥ 0.001 pu to avoid numerical problems.

2.2.5 Symmetric and asymmetric ZIP models

We use two different ZIP models to represent 3-phase aggregated loads and generations. An asymmetric ZIP model, which models each phase of the device independently, and a symmetric ZIP model, which has the same set of ZIP parameters on all phases.

Asymmetric ZIP model: the ZIP equivalent circuits of each phase are independent and can thus have different sets of ZIP parameters. For each phase, we use a 1-phase PLL to estimate the frequency and phase of the corresponding phase voltage. Each PLL is controlled by a PI-controller and has two dynamic parameters, K_p and K_i, which need to be identified. The magnitude of each phase voltage is also estimated to be able to adapt the current drawn by the constant power source. We use the magnitude estimation and the PLL model implemented in the Variable static load device of the EMTP library [5].

Symmetric ZIP model: this model has one set of parameters used on all the phases. Additionally, it is synchronized to the positive sequence component of the node voltage. This ensures that the currents drawn by the I- and S- branches on different phases are always symmetric with the same amplitude. The impedance of the ZIP model is also symmetric. The double-decoupled synchronous reference frame Phase Locked Loop (DDSRF-PLL) described in [6] based on the Park transformation is used to estimate the magnitude, phase and frequency of the positive sequence voltage.

2.3 Innovative method for ZIP model parameter identification

2.3.1 Identification method

Our goal is to represent the aggregated loads and generations at grid nodes using the ZIP model. Using the ZIP models at each node, we can perform a short-circuit analysis that accurately computes the short-circuit currents in the grid, taking into account also the short-circuit current contribution of distributed generation.

The model parameters are determined using a time-domain identification procedure that uses measurement data. We use data related to a variation of current absorbed/generated at the grid node due to sudden voltage variations, which can be caused by various events occurring in a real grid, such as the operation of an On Load Tap Changer (OLTC). The ZIP model needs to be accurate during steady-state and also faulty conditions, indeed we use a time-dependant ZIP model including the dynamic reaction of the component to voltage changes.

We use EMTP to simulate such voltage steps and to record the reaction of the loads and generators in terms of variation of absorbed/generated current. The following devices are considered:

- a pure impedance load consuming 100 kW and 40 kVAr at nominal voltage,
- a Photovoltaic Power station (PV) generating 2 MW (very detailed model provided by EMTP),
- aggregations consisting of a PV and an impedance load connected via a transformer to the MV network.

We designed a least squares optimization method to identify the parameters of the asymmetric and symmetric ZIP models. The results from identified devices are presented in Section 3.3 and the use regarding short-circuit analyses in Section 3.4.

2.3.2 Performance evaluation metric

We perform fault simulations in EMTP to evaluate how accurately each ZIP model is representing the short-circuit currents of the identified devices. We use a distribution network at 11 kV (RMS value of the line-to-line voltage) where we connect the reference devices or ZIP models to a certain bus and perform simulations of faults on the line exiting the bus. The network is supplied by a HV/MV transformer with 20 MVA nominal power.

For each simulation, either a reference device or a ZIP model is connected to the bus. The node voltage and current injections at the node are recorded and compared. We use symmetrical faults as shown in Figure 3 with R_f equal to 1 and 10 to cover the most frequent faults occurring in a distribution grid. The fault inception angle is set to 0, which corresponds to the zero-crossing of the rising sinusoidal voltage waveform in phase A.

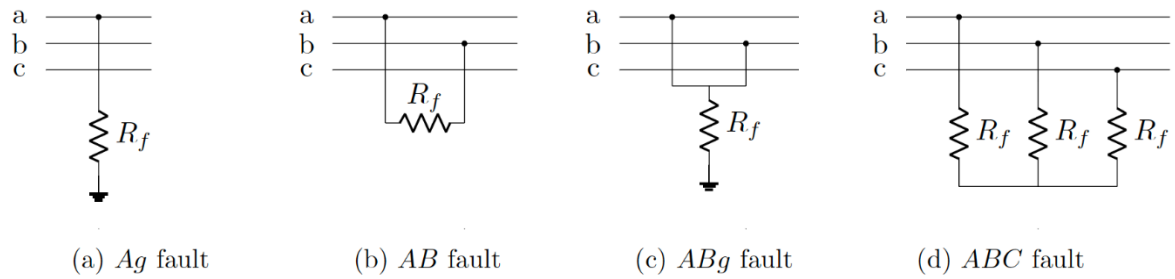

Figure 3 – Considered faults with symmetric fault resistances.

To evaluate the current matching, we use the nRMSE as defined in Eq. (3) with $y = i_{ref}$ and $\hat{y} = i_{zip}$. The normalization is related to the energy contained in the reference signal. The error is evaluated for all phases and using only data during the fault. The final nRMSE showing how good the ZIP model is representing the reference device is the average over the nRMSE values of the faulty phases. If i_{ref} and i_{zip} match perfectly, the nRMSE equals 0, which is the lower bound. If the error equals 1, the matching of the currents is bad and not better than setting $\hat{y} = i_{zip} = 0$. The nRMSE metric has no upper bound. For values above 1, i_{ref} and i_{zip} do not match at all.

$$nRMSE(y, \hat{y}) = \sqrt{\frac{\sum_{n=1}^{N}(y_n - \hat{y}_n)^2}{\sum_{n=1}^{N} y_n^2}} \tag{3}$$

2.4 Assessment of the existing protection system

Once the grid models were ready to be simulated in EMTP-RV, DG has been progressively added to the MV feeders to reproduce the share of PV generation targeted by the Canton of Geneva for 2030. The maximum power generated by DG in a single feeder was chosen to be of about 12 MW (350 MW of installed nominal power leads to roughly 40 MW associated to each of the 8 primary substations, to be shared among the various MV feeders fed by the substation). A parametric analysis varying DG location, fault location, fault impedance as well as fault type (symmetrical / asymmetrical) has been performed to determine which cases might produce a malfunction of the protection relays. The results of these simulations are detailed in the sections below.

Overcurrent (OC) protection

In case of a fault that produces high short-circuit currents, instantaneous overcurrent relays (ANSI 50) are installed at the root of each feeder departing from the primary substation. The instantaneous OC protection is set to: I_{max} = 1000 A and t = 50 ms.

Overload protection

Even though overload situations are characterized by less severe current levels than in the case of short-circuits, the temperature rise due to extended overload conditions is just as likely to cause cable failure.

The overload protection curve (ANSI 49) is shown in blue in Figure 4 and can be expressed as follows:

$$\Delta t = 100\% \cdot \frac{I^2}{I_{rated}^2} \cdot (1 - e^{-t/\tau}) \tag{4}$$

where $I_{rated} = 250\,A$ and $\tau = 60\,min$.

This protection curve can be compared with the thermal rating curve of a cable, as shown later in Figure 8.

In addition to including models for each component of the power system, EMTP-RV offers a built-in library containing standard protection functions such as overcurrent or overload ones. However, since the trip (or alarm) condition is basically exceeding a current threshold during at least a certain time, the modeling of the overcurrent (and overload) relay in EMTP-RV is not necessary for the present study.

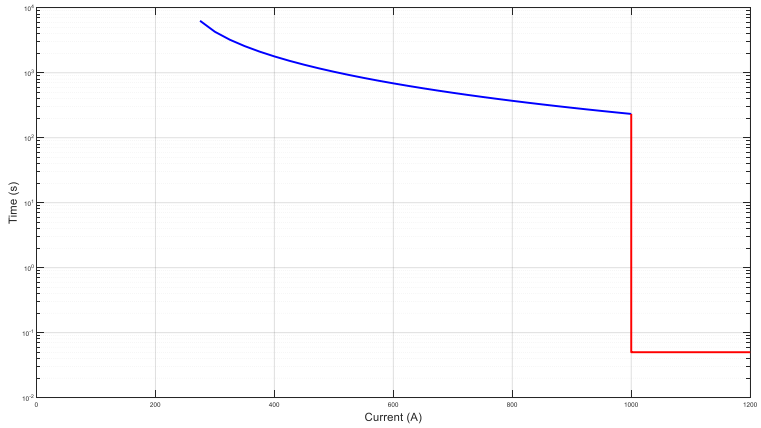

Figure 4 - Protection settings at the root of the feeders (Blue: Overload; Red: Instantaneous overcurrent)

An assessment of the robustness of the existing protection strategy has been performed using the models mentioned above. Two distinct types of faults are considered: symmetrical faults (which tend to produce the highest currents) and single-phase-to-ground faults. Among the asymmetrical faults, in fact, only the case of one phase to ground is of interest because of its challenging detection because of the Petersen coil (as discussed in Section 2.1) and is supposed to be detected by the directional earth-fault protection relay. The remaining asymmetrical cases (phase-to-phase faults) produce significant fault current levels, of the same order of magnitude of the symmetrical ones, thus the same considerations apply.

2.4.1 Symmetrical faults

In our case, the fault clearance of symmetrical faults (three-phase fault scenarios) is the competence of overcurrent protections. Therefore, two major threats associated with DG were simulated, namely 'blinding' and 'sympathetic tripping' (see their schematic explanation in Figure 5). To find the vulnerabilities of the protection system currently in operation, we performed a parametric analysis by changing the position of the PV as well as the fault location, as shown later in Figure 7.

Blinding
A first threat associated to DG installed on a feeder already protected by an overcurrent relay is the so-called 'blinding' case, in which the DG feeds a short-circuit occurring on that same feeder, hiding the actual fault current amplitude from the protection relay. This results in an undetected fault or delayed tripping which would inevitably damage or even burn some cables.

Sympathetic tripping
The second threat that has been considered associated to DERs is the so-called 'sympathetic tripping', in which the DG installed in a certain feeder feeds a short-circuit occurring on a different feeder, via the common busbar at the MV transformer level. If the protection relay has not the directional feature, the relay in the healthy feeder might trip if the current supplied by the DG exceeds the overcurrent threshold.

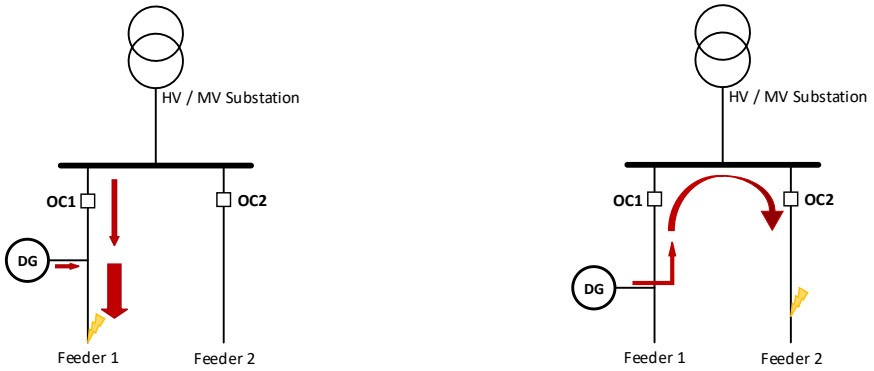

Figure 5 – Illustration of a blinding caused by the DG (left) and a malfunction leading to sympathetic tripping (right)

2.4.2 Single-phase-to-ground faults

The EMTP-RV model of the directional earth fault protection has been designed according to the indications provided by the DSO and its behavior has first been validated, as shown below.

The validation has been performed assuming the faulted topology indicated in Figure 6 with a single-phase ground fault occurring at the end of Feeder 78, characterized by a fault resistance of 0.1 Ω.

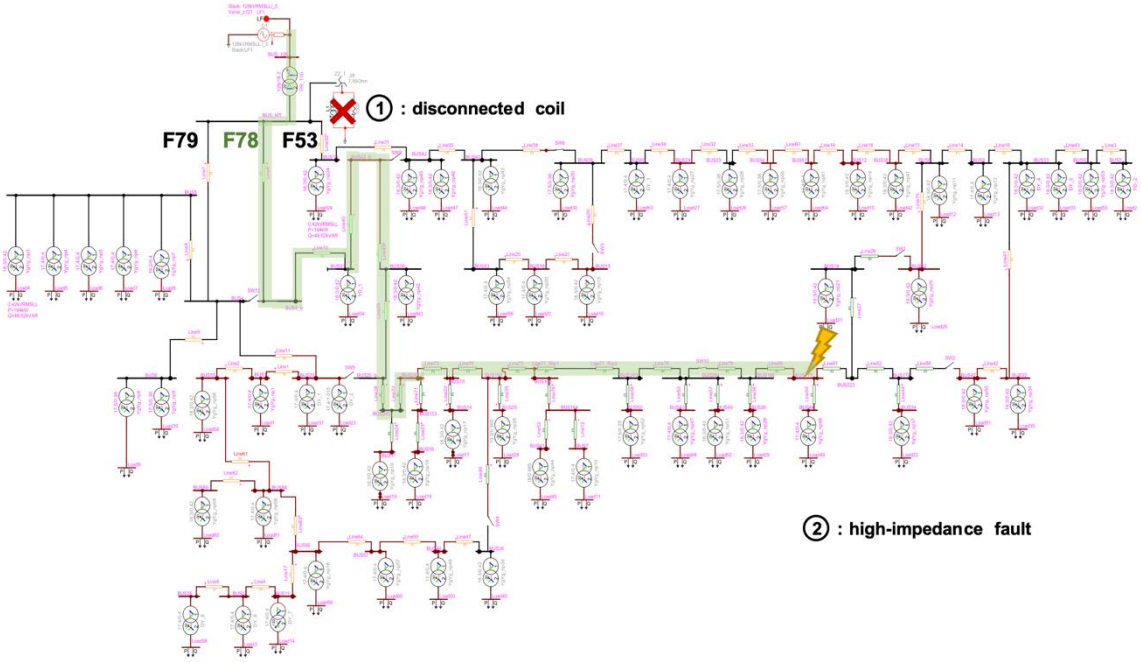

Figure 6 - Single-phase-to-ground fault scenario that led to a malfunction of the directional earth-fault protection.

Figure 7 shows the current and voltage phasors as measured by the protection relays installed on the roots of the three feeders. As expected, the angle difference between I_0 and U_{ref} is about 90° on both healthy feeders and should be close to 0° on the faulted feeder [7].

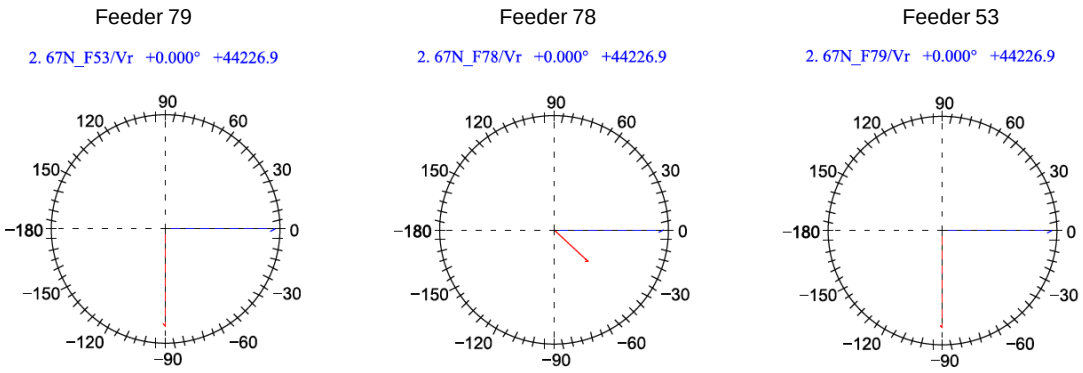

Figure 7 - Current and Voltage phasors during the fault for all feeders

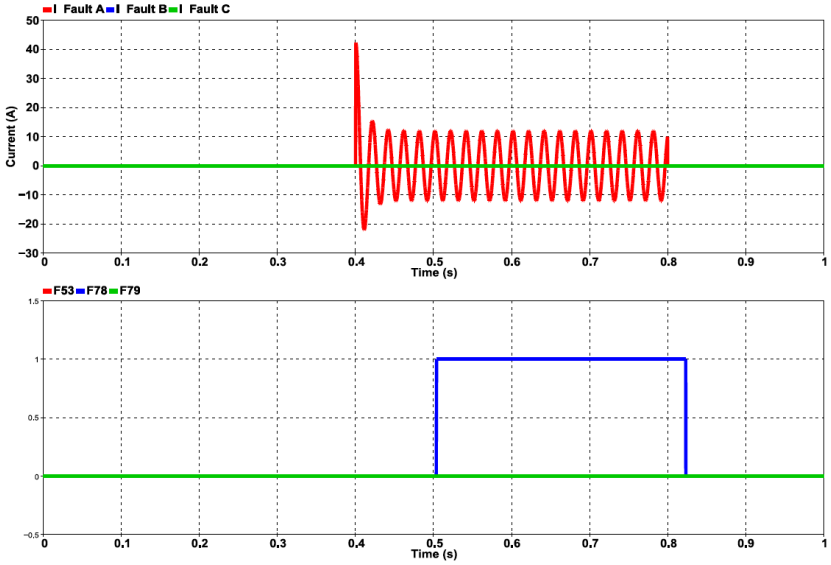

Figure 8 - Fault current and tripping signals from the protection relay

As already mentioned, to reduce the simulation time, the tripping time delay was set equal to 100 ms rather than the actual value of 1000 ms implemented in the relay. Figure 8 shows that only the faulted feeder (F78) is warned by the protection scheme.

According to [8], PV power plants do not represent a threat during single-phase fault because they are not connected to the ground at the medium voltage level (so they do not influence the zero-sequence impedance). Therefore, no DG is included in the following simulation.

2.5 Development of an adaptive protection strategy

The idea of the adaptive scheme is to run a thorough short-circuit analysis to define offline a certain number of scenarios (e.g., high PV production or low PV production) and calculate the values of the parameters for each setting group to be pre-charged in the relays. The grid controller would then select the more adequate setting group according to the real-time observation of the grid.

2.6 Validation in a real-time HIL simulation environment

Real-time simulation is the proper tool to be used when assessing the performance of a protection algorithm, to correctly assess the response time of the calculations. Coupling the real-time modeling with Hardware-In-the-Loop environment allowed us to properly evaluate the physical latencies of all the processes in the chain.

3 Results and discussion

The results obtained in the different work packages of the project are illustrated hereafter.

3.1 Robustness against severe faults (three-phase and two-phase faults)

The feeder F78 has been considered for the following analysis because of its larger impedance leading to smaller short-circuit currents for typical values of fault impedance (a few Ohms). Its considerable length, as well as its mixed buried-overhead topology, also provides many interesting potential fault locations. It is also worth mentioning that a biogas power plant is planned to be installed along this feeder, which also favors its choice for the parametric analysis.

Assuming a total PV power of 12 MW (equally shared among three 4-MW plants), the parameters adopted for this analysis are:

- fault location (four different locations chosen along the feeder)
- fault resistance (values varying from 4.5 Ω to 10 Ω)

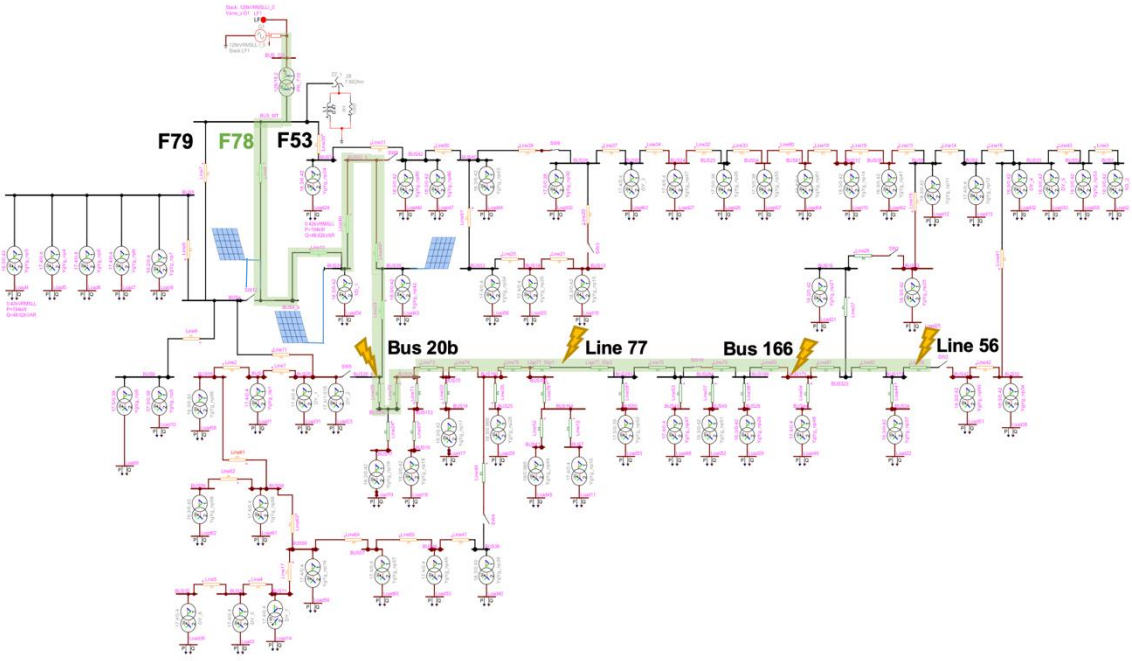

Figure 7 - Schematic representation of the parametric analysis of symmetrical-fault scenarios performed for Feeder 78

As mentioned above, the blinding effect is caused by a current contribution coming from DG along the feeder that hides the true amplitude of the fault current from the protection relay. This means that, even though the current seen by the relay increases, it may not be high enough to make the instantaneous OC protection trip. However, the current being higher than the rated current (namely, 250 A_{rms} for the cables considered here), the overload function will trip after a certain delay, determined by the blue curve of Figure 4. Now, depending on the actual current flowing through the cable, the latter may burn before the protection trips.

The time needed to burn a cable can be determined using Eq. (5):

$$I^2 \cdot t_{max} = K^2 \cdot S^2 \tag{5}$$

where:

I is the current flowing through the cable in A
K is a coefficient depending on the type of insulation in A·s/mm^2
S is the section of the cable in mm^2

Assuming for our case a value of 143 for the coefficient *K* (the cable insulation is assumed to be XLPE) and a cable section of 150 mm^2, the relation between time and maximal admissible current of the cable can be determined and is shown in red in 8. The blue curve is the overload tripping characteristic of the relay, already defined in Eq. (4) and depicted in Figure 4.

Figure 8 illustrates the risk associated to the blinding mechanism. A given overload current measured by the protection relay at the feeder root (950 A_{rms} for instance) is set to be cleared before a certain time in order to avoid a cable failure (namely, 258 s). In case of blinding, close to the fault location the current level is increased because of DG contribution. If this level exceeds the maximal admissible current that can flow through the cable for 258 s continuously (namely, 1334 A_{rms}), the cable will be damaged or burnt before the overload protection trips.

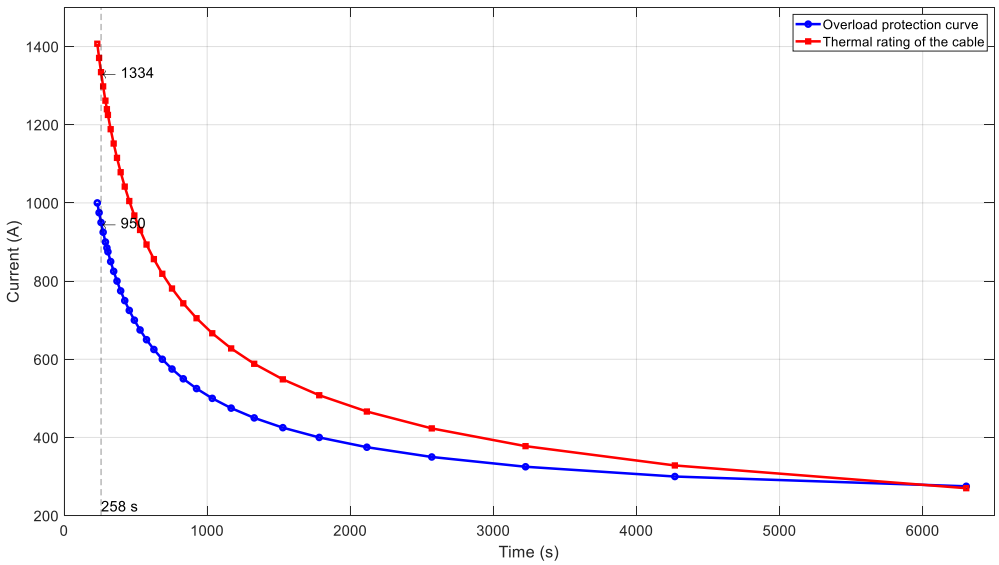

Figure 8 - Maximal admissible current for the cable (red) and overload protection function (blue).

Figure 9 shows the occurrence of blinding situations as function of fault resistance and fault location, after a parametric analysis as discussed. The fault cases in which the DG would blind the protection relay are contained within the yellow areas. Those highlighted areas are bound by the instantaneous OC protection settings on one side (where I_{feeder} > 1000 A) and by the proper functioning of the overload protection on the other side.

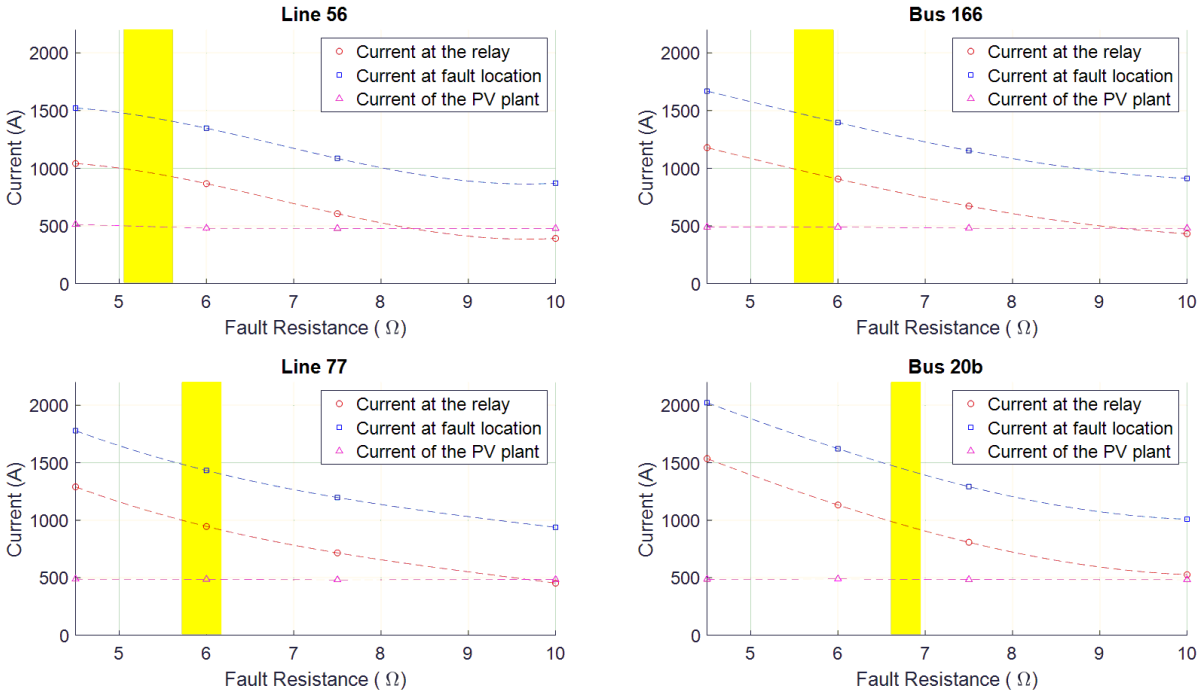

Figure 9 – Blinding occurrence as a function of the fault resistance (highlighted in yellow)

Furthermore, a scenario including a 3-MW biogas plant is considered. This is of interest because such a plant is actually going to be installed at the location shown in Figure 10 and its short-circuit contribution could be larger than the one provided by static converters like the ones installed at PV plants if the fault location is close to it. The biogas plant has been modelled as a synchronous machine with its exciter. There is also a transformer between the plant and the MV grid.

It has to be noted that no occurrence of sympathetic tripping has been found for reasonable values of DG power (maximum 12 MW of PV nominal peak power per feeder) after a parametric analysis performed on all the sections of the MV network that have been considered.

Parameters adopted for this scenario:

Faulted feeder: F78
Feeder hosting PV: F78
DG: 1x 6 MW (PV) + 1x 3 MW (biogas)
Fault type: ABCg
Line impedance (from busbar to fault location): 1.7 Ω
Fault resistance: 6 Ω

Using the results of the analysis above, the fault resistance is set to 6 Ω to be in the blind range of the protection when the fault is located on Bus 56. This time however, since a biogas plant is located close to the fault, only half of the PV is installed on the faulted feeder. This choice of reducing the amount of PV is mostly due to the amount of current that would flow through the lines close to the begging of the feeder during normal operation if 3 MW of 12 MW of PV we both installed on the same feeder. It will lead to unrealistic scenarios considering the current topology of the MV network.

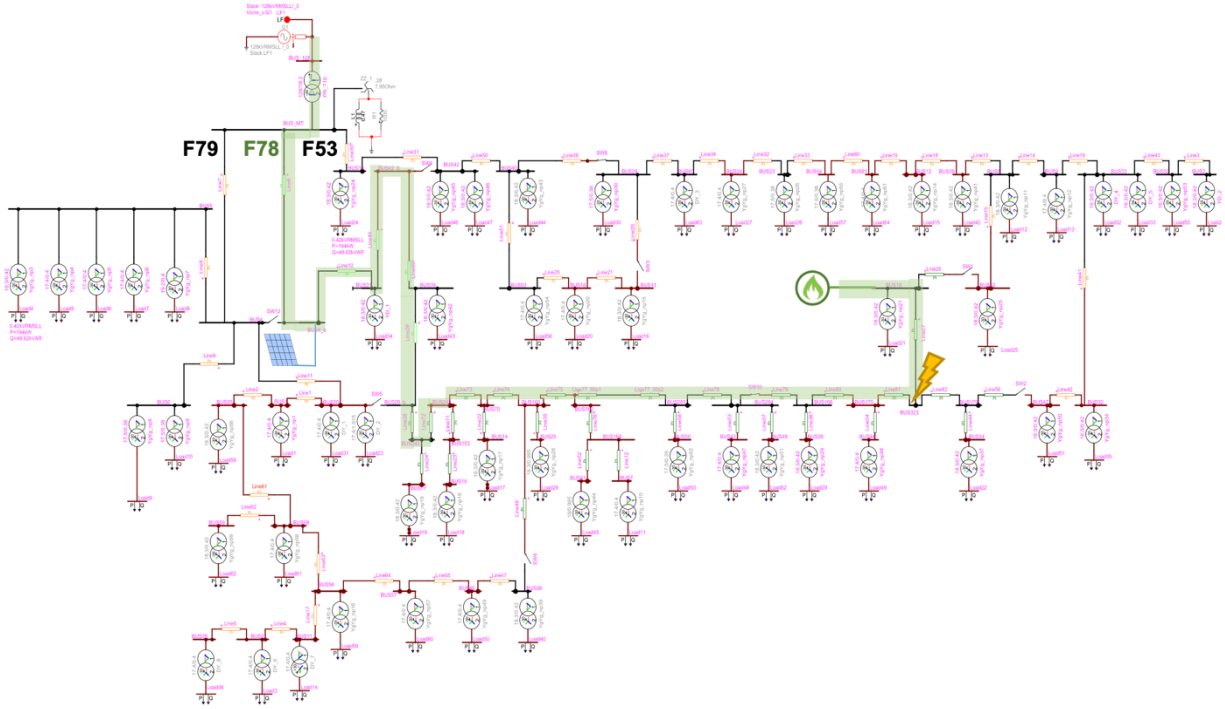

Figure 10 - Location of the biogas power plant and the simulated fault

The results of the simulation presented above are shown in Figure 11 (RMS values listed in Table 1). A 6 MW PV plant is located close to the root of the feeder and the fault is located close to the 3-MW biogas plant. The result is similar to the previous simulations that only included PV. The protection does not trip while the cables close to the fault will burn before the thermal protection detects it.

In this case, 6 MW of PV are enough to create the blinding; this is due to the behavior of the rotating machine which produces twice its rated current to support a fault that is located close to it.

The addition of a biogas plant still does not create sympathetic tripping issues since this DG is located far enough from the transformer MV busbar. In case of fault on a different feeder, in fact, the fault-current contribution of the DG will be limited by the relatively high cumulated impedance of the lines between the root of the feeder and the biogas plant location (~1.5 Ω).

The other selected portions of the MV grid referring to different primary substations have been assessed against 'blinding' and 'sympathetic tripping'. A parametric analysis has also been performed and the results are shown in Appendix 3.

Table 1 – RMS current values corresponding to the time-domain curves shown in Figure 11

	Before fault	During Fault
Feeder-root current (A_{rms})	350	987
Fault current (A_{rms})	-	1400
PV-plant current (A_{rms})	230	230
Biogas-plant current (A_{rms})	105	183

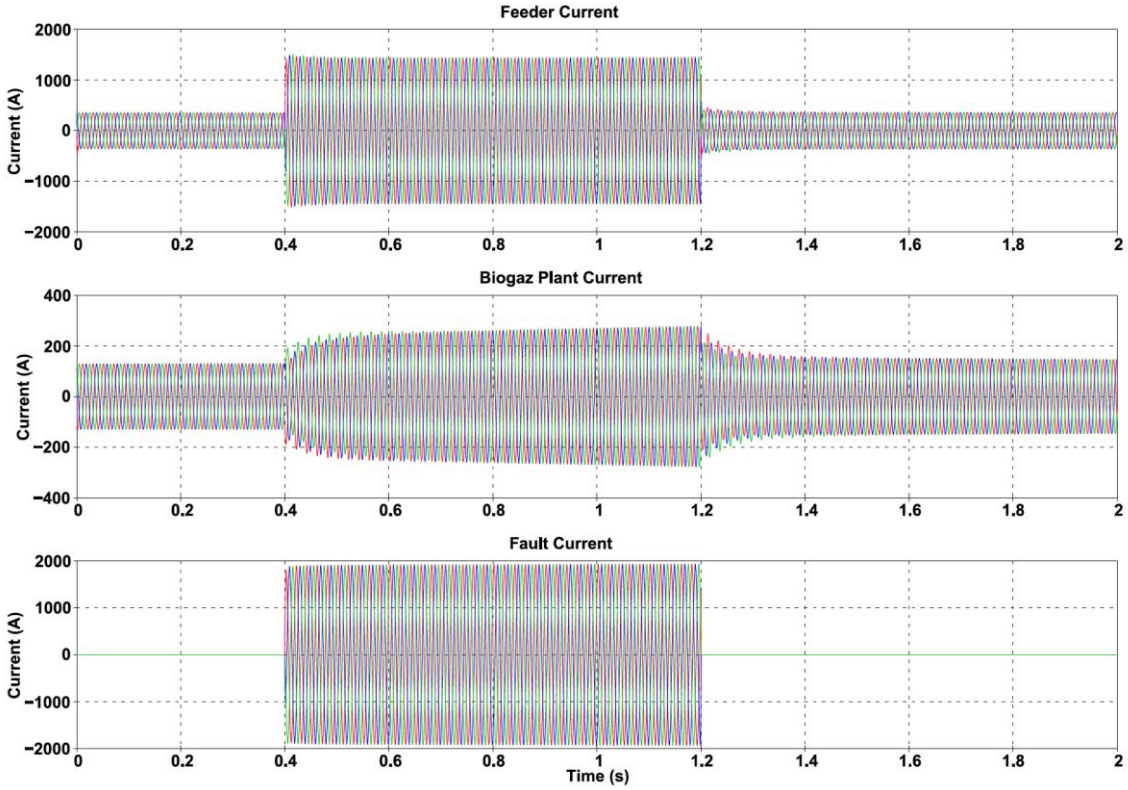

Figure 11 - Impact of the biogas on the fault current (Red: phase a; Blue: phase b; Green: phase c)

Top: Current measured by the protection; **Middle**: Current injected by the DG; **Bottom**: Current in the faulted line

Recommendations for severe faults (three-phase and two-phase faults)

A first recommendation would be to reduce the threshold of the instantaneous overcurrent function. According to the parametric analysis performed, in fact, the lowest current measured at the feeder root by the protection relays is around 910 A, which suggests that an instantaneous OC threshold lowered to 800 A (instead of 1000 A) would allow clearing the risk of blinding.

A second recommendation could be to add a time-delayed OC function (ANSI 51) to the characteristics shown in Figure 4. Having a second step of overcurrent protection set between 800 A and 900 A and t = 1 s would also clear the risk of blinding.

3.2 Robustness against single-phase-to-ground faults

In order to evaluate the performance of the directional earth fault protection, several simulations on the same network were performed. We identified two fault scenarios (depicted as 1 and 2 in Figure 6) where the directional earth-fault protection was unable to detect the single phase-to-ground fault:

- Case #1: 0.1-Ω single-phase ground fault occurring at the end of Feeder 78 and Petersen coil disconnected.

  A malfunctioning of the Petersen coil might cause the network grounding to switch from compensated to isolated. Without a quick adaptation of the protection settings for isolated networks, the relay is not able to identify the fault (as shown in Figure 12).

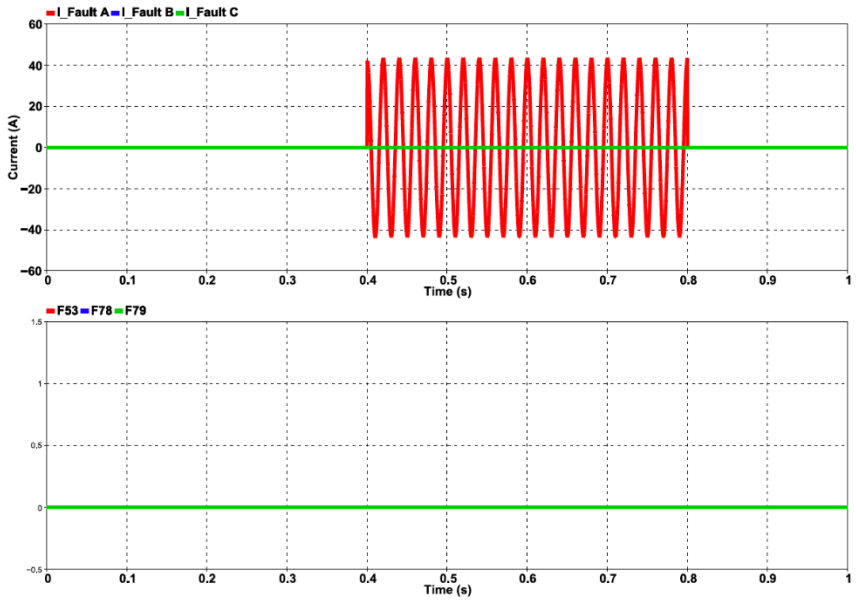

Figure 12 – Fault current and tripping signals in case of failure of the Petersen coil using the same algorithm as above

As a possible solution to improve the behavior of the protection relay in case of malfunctioning of the Petersen coil, an $I_0 sin\varphi$ logic could be adopted instead of the $I_0 cos\varphi$ one currently in use. Figure 13 shows that with the new algorithm, the protection is able to detect the fault, even if the MV network is now isolated from the ground.

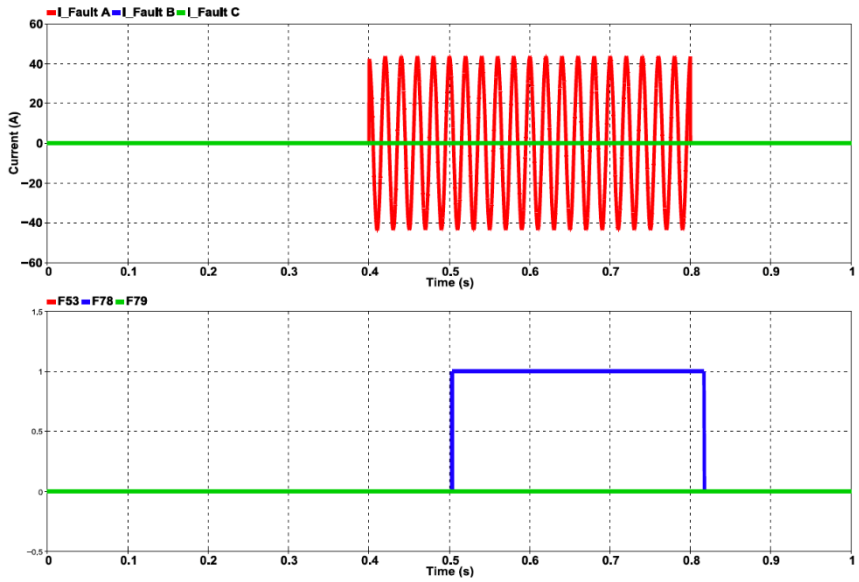

Figure 13 – Fault current and tripping signals from the protection relay using the $I_0 sin\varphi$ algorithm

- Case #2: high-impedance (1.5 kΩ) single-phase-to-ground fault at the end of Feeder 78 with Petersen coil in service.

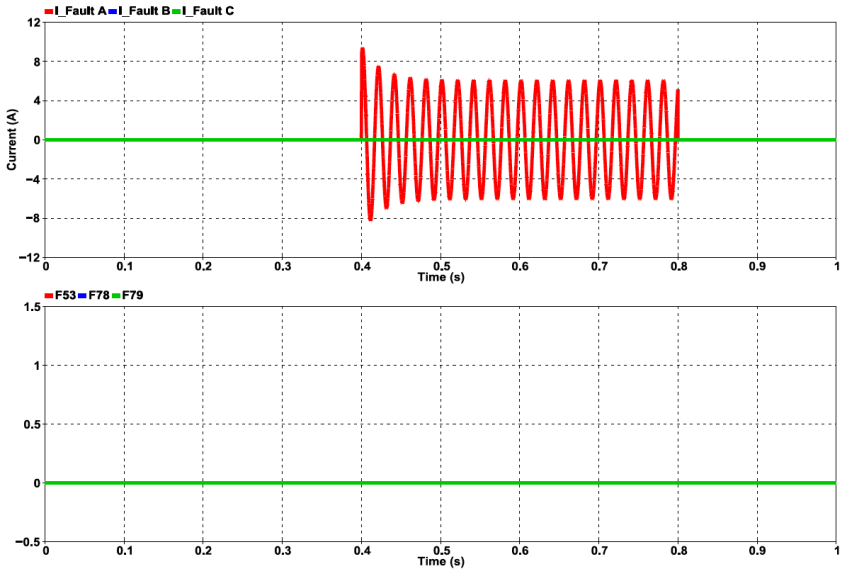

Figure 14 – Fault current and tripping signals in case of high impedance fault

For the topology investigated in Case #2, the maximum fault impedance value which the relay is capable of detecting is slightly less than 1.5 kΩ. As shown in Figure 14, the relay was not able to detect a fault characterized by such high impedance.

Figure 15 shows that when the threshold for the residual voltage is set to $0.15 \cdot U_n$ instead of $0.4 \cdot U_n$ the relay is able to detect high impedance faults.

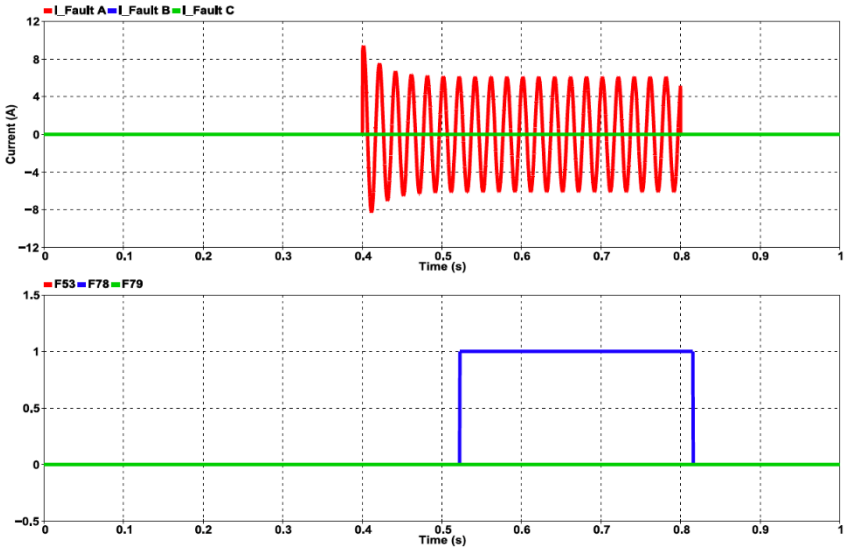

Figure 15 – Fault current and tripping signals from the protection relay during high impedance faults using smaller thresholds

Recommendations for single-phase-to-ground faults protection settings

- The thresholds of $3U_0$ and $3I_0\,cos\varphi$ should be lowered if even these types of fault need to be detected.
- Instead of $3I_0\,cos\varphi$, the logic $3I_0\,sin\varphi$ would be more robust (e.g. in case of Petersen coil's failure)
- Other algorithms, like *Wischer* or *qu2,* tend to offer better performances than the classic $3I_0\,cos\varphi$ one and their performances would not depend on the neutral grounding scheme.

The remaining selected portions of the MV grid referring to different primary substations (whose topology is shown in the Appendices) have also been assessed against high-impedance single-phase-to-ground faults, showing that the considered relays are not able to detect faults whose impedance is higher than 4.4 kΩ.

It has to be noted that the present study does not take into account the case of intermittent earth faults. Solving the tricky problem of their detection goes beyond the scope of this study and is left to an option in case the project schedule would leave resources for that.

3.3 Results of ZIP parameter identification of load and generation

In this section, results are presented for the identifications of an impedance load, a PV and aggregations composed of impedance loads and PVs as mentioned in Section 2.3.

We use data which are 400 ms long and which contain symmetric voltage steps of 3%, 10% and 30%. A 3% voltage drop happens quite frequently in the grid due to the operation of the OLTCs. Steps of 10-30% are less frequent but still occur from time to time. We thus use data which could be recorded from the normal operation of a distribution grid. For each dataset, both asymmetric and symmetric ZIP models are identified. The performance will be assessed as described above.

The approach of finding a good coarse parameter grid is shown for the PV device. The motor convention is used to specify the powers consumed or generated by a load.

3.3.1 Identification of a load composed by a pure impedance

We first perform ZIP identifications of a pure impedance load consuming 100 kW and 40 kVAr at a nominal voltage of 11 kV (RMS line-to-line value) to show the convergence of our approach. The load is directly connected to the network at 11 kV, where a 10% voltage step occurs.

The nRMSE between i_{ref} and the ZIP current is below 0.006 for both ZIP models and for all phases. As expected, the value is very low and shows that the optimization problem was solved successfully with a low final objective value. It means that the identified ZIP model outputs currents very close to i_{ref} if the ZIP node voltage equals v_{ref} .

Table 2 compares the identified values of R and L to the true values inferred from the data. We see that the impedance could be well identified, as the error always lies below 10 %. The symmetric ZIP model even achieves a very good matching of the impedance load. The errors in the estimation of the true R and L is not bigger than 0.1% and the contribution of the I- and S-branches is practically 0.

The time-domain performance of a ZIP representing an impedance load in faulty conditions will be analysed in Section 3.4.

Table 2 – Impedance matching for the ZIP identification of a pure impedance load. The columns e_R and e_L show the relative errors

		R [Ω]	L [H]	R_{zip} [Ω]	L_{zip} [H]	e_R [%]	e_L [%]
asymmetric ZIP	phase A	1206	9.63	1260	9.60	4.5	0.3
	phase B	1206	9.63	1273	9.32	5.6	3.2
	phase C	1206	9.63	1210	10.55	0.3	9.6
symmetric ZIP		1206	9.63	1206	9.62	0.0	0.1

3.3.2 Identification of a photovoltaic power station

We use the PV model available in EMTP-RV [5] generating 2 MW. The power plant is connected to the MV grid via an DC/AC converter and a step-up transformer. The model has a FRT capability such that it does not disconnect itself during voltage sags lasting for less than 0.1 s. It will thus stay connected during the faults we are simulating (which last for 80 ms). The identification of the PV takes into account the whole chain including the total of the actual solar cells, the converter and the step-up transformer.

We performed identifications of the PV using a symmetric ZIP model and data containing a 10% voltage step. For this device, we also assessed the performance for identifications using the different voltage steps in the data (3 %, 10% and 30 %).

We finally get 2 different ZIP equivalents, an asymmetric and a symmetric ZIP model, for each dataset. They all have a nRMSE value below 0.05 when comparing the ZIP currents of all phases to i_{ref} from the identification data. It means that the optimization problem solved for each ZIP model has a low final objective value and that the identified ZIP models output currents very close to i_{ref} if the ZIP node voltage equals v_{ref} .

We perform fault simulations as described in Section 2.3.2. The reference device and the six ZIP equivalents are successively connected to the bus in the network close to the fault, and the voltage and current waveforms are recorded. Table 3 shows the voltage drops occurring at the bus for the different faults and devices. The columns for 2-phase faults show the voltage drops in phases A and B. The values are very similar, meaning that the different ZIP devices and the reference device experience practically the same voltage drops.

Table 3 – Voltage drops during faults for simulations with different ZIP equivalents of the PV.

	ABC		AB		ABg		Ag	
	1Ω	10Ω	1Ω	10Ω	1Ω	10Ω	1Ω	10Ω
reference	33 %	4 %	19 %/57 %	1 %/10 %	59 %	51 %	33 %	4 %
asymmetric ZIP 3 %	33 %	4 %	19 %/57 %	1 %/10 %	59 %	50 %	33 %	4 %
symmetric ZIP 3 %	33 %	4 %	19 %/57 %	1 %/10 %	59 %	50 %	33 %	4 %
asymmetric ZIP 10 %	33 %	4 %	18 %/57 %	1 %/10 %	58 %	50 %	33 %	4 %
symmetric ZIP 10 %	33 %	4 %	19 %/57 %	1 %/10 %	59 %	50 %	33 %	4 %
asymmetric ZIP 30 %	33 %	4 %	19 %/57 %	1 %/10 %	58 %	50 %	33 %	4 %
symmetric ZIP 30 %	33 %	4 %	19 %/57 %	1 %/10 %	59 %	51 %	33 %	4 %

Table 4 – nRMSE of the fault current absorbed by the identified ZIP models with respect to the reference PV.

	ABC		AB		ABg		Ag	
	1Ω	10Ω	1Ω	10Ω	1Ω	10Ω	1Ω	10Ω
asymmetric ZIP 3 %	0.17	0.09	0.44	0.09	0.87	0.94	0.37	0.07
symmetric ZIP 3 %	0.45	0.07	0.31	0.07	0.86	0.76	0.08	0.02
asymmetric ZIP 10 %	0.23	0.08	0.60	0.11	1.34	1.26	0.50	0.07
symmetric ZIP 10 %	0.44	0.07	0.31	0.07	0.85	0.75	0.07	0.02
asymmetric ZIP 30 %	0.13	0.07	0.46	0.09	0.99	1.02	0.37	0.07
symmetric ZIP 30 %	0.24	0.08	0.14	0.07	0.24	0.21	0.08	0.02

Table 5 – Powers absorbed by each branch of different symmetric ZIP models of the PV generating 1990 kW and absorbing 99.9 kVAr.

	P_n [kW]	Q_n [kVAr]	S_Z [kVA]	S_I [kVA]	S_S [kVA]	S_{tot} [kVA]
3%	-1990.0	99.9	0.1-95.2i	-21.1-24.1i	-1970.4+220.1i	-1991.4+100.8i
10%	-1990.0	99.9	0.1-109.0i	-48.8-68.9i	-1941.6+278.8i	-1990.3+101.0i
30%	-1990.0	99.9	0.1-130.5i	-1462.6+88.2i	-528.2+144.4i	-1990.6+102.2i

Table 4 shows the nRMSE values when comparing the currents of the different ZIP equivalents to the reference current (average nRMSE over the faulty phases). Regarding the 3-phase fault, we can observe three things. First, the matching is really good for small voltage drops. The errors for the ABC 10Ω are very low, but the voltages drop only around 3% when this fault occurs. Second, the asymmetric ZIP model achieves a better matching for bigger voltage drops. For these models, the matching is also good for the ABC 1Ω fault. Third, the performance improves for the symmetric ZIP model when the data used for the identification contains bigger voltage drops.

Regarding asymmetric faults, the errors are much smaller for the symmetric ZIP equivalent. For Ag and AB faults, the nRMSE values stay below 0.3. For the Abg fault however, the errors are big and the matching is only good when using the symmetric ZIP model and a 30% voltage drop in the identification data. The performance is worst during Abg faults because they cause the biggest voltage drops (see Table 3). If the voltage at the node deviates more from nominal conditions, we are further away for the data used in the identification and it is clearly not guaranteed that the identified ZIP model is also valid in that voltage range. Figure 15 and Figure 16 show the currents of the asymmetric and symmetric ZIP models during Abg 1Ω faults for identification using a 3% and 30% voltage drop respectively, illustrating the improved performance when using data with more voltage variations. We show the voltage matching for one ZIP model only, as the voltage drops are very similar for all ZIP equivalents and for the specific fault.

Comparing the currents from the symmetric and asymmetric ZIP model in Figure 16a and Figure 16b we can see that the error is higher for the asymmetric model because the current waveforms are shifted with respect to the reference. In the asymmetric ZIP model, the current and power sources of each phase are synchronized to the respective phase voltages. So for a Abg fault, where the voltages in phase A and B shift in phase and overlap, the currents of the I- and S-branches also shift in phase. The true PV plant however always outputs symmetrical currents. Hence, the symmetric ZIP model with symmetric constant current and constant power generators is much more suited to represent the PV during asymmetric faults and achieves a better matching for those cases.

Table 5 shows the branch powers of the symmetric ZIP equivalents obtained with the different data sets. We see that more power is assigned to the I-branch and less power to the S-branch for identification data with bigger voltage steps. During fault simulations it has the effect that the amplitude of the total current increases less for the same voltage drop. We can see this effect comparing Figure 15b to Figure 16b, which show the currents during Abg faults for the symmetric ZIP model identified with a 3% and 30% voltage drop, respectively.

The overall performance is better for the symmetric ZIP model identified using a 30% voltage drop, because it can limit the mismatch more during large voltage drops as the S-branch of this ZIP model is less important.

Summarizing, we can well represent a PV for symmetric grid conditions using the asymmetric ZIP model and data with only very small voltage steps. When doing short-circuit analyses with asymmetrical faults, the symmetric ZIP equivalent achieves a better matching as it outputs symmetrical currents as the reference device also does. To achieve more accurate representations over a wider range of voltage steps, we do however need deeper voltage drops in the identification data.

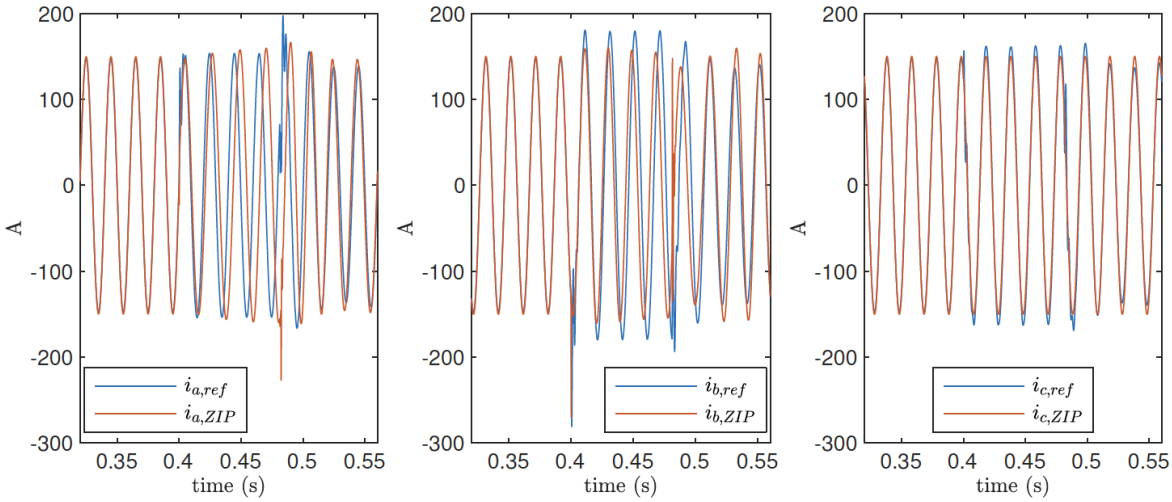

(a) Currents of the reference and the asymmetric ZIP model.

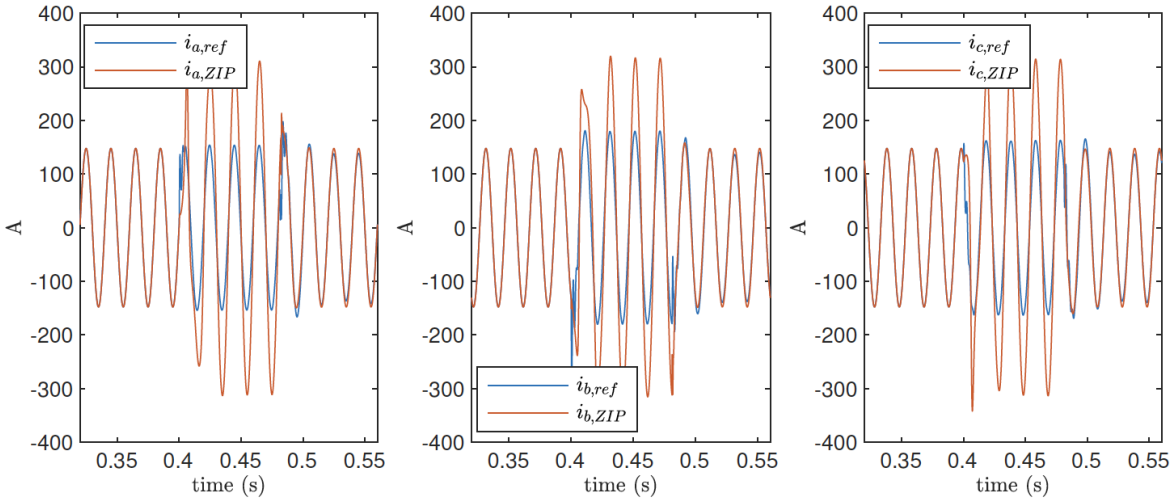

(b) Currents of the reference and the symmetric ZIP model.

Figure 15 – Comparison for the Abg 1Ω fault using data with a 3% voltage drop to identify the PV.

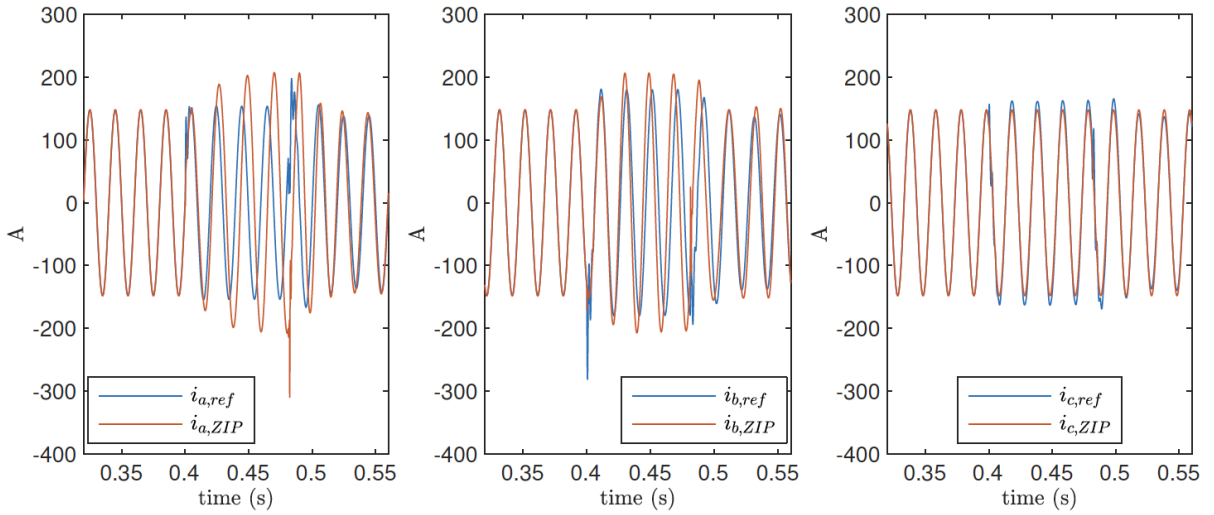

(a) Currents of the reference and the asymmetric ZIP model.

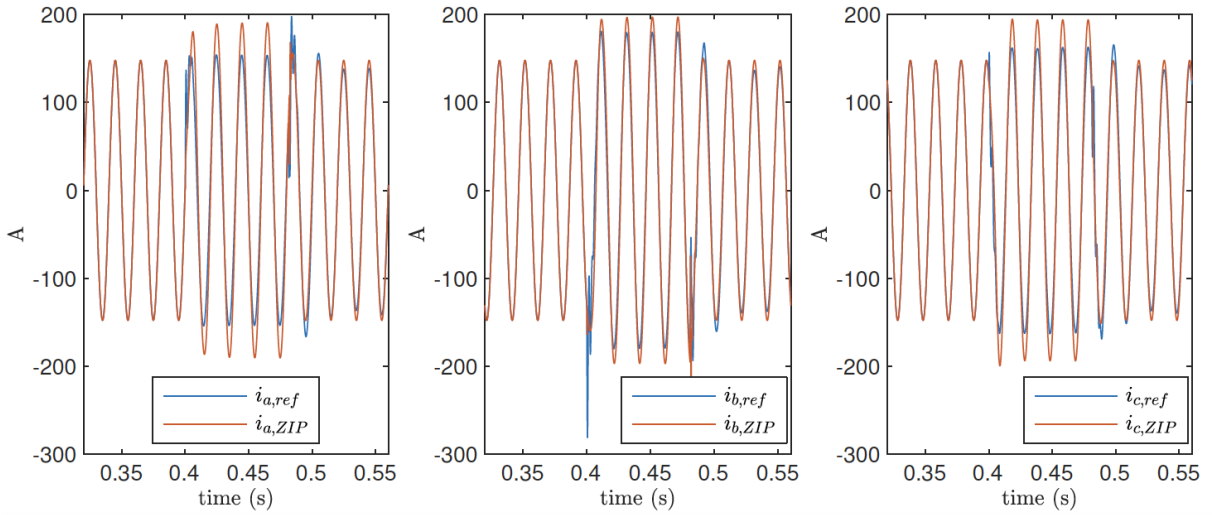

(b) Currents of the reference and the symmetric ZIP model.

Figure 16 – Comparison for the Abg 1Ω fault using data with a 30% voltage drop to identify the PV.

3.3.3 Identification of aggregations of loads and generations

We consider two different aggregations of a load and a generation unit. The structure of both is shown in Figure 17. The impedance load L is connected to the grid via a Dy transformer at 11/0.42 kV (RMS line-line values). The two considered cases are:

- Case A: The PV is generating 2 MW and the impedance load has a nominal power of 4 MW with a power factor of 0.9.
- Case B: The PV generates 8 MW and the load consumes 1 MW at nominal voltage with a power factor of 0.9.

For both cases, we assess again the performance of different identified ZIP equivalents. Three data sets containing voltage drops of 3%, 10%, and 30% are used per device to identify both asymmetric and symmetric ZIP models.

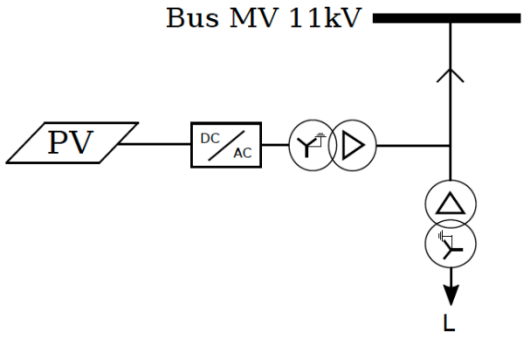

Figure 17 – Aggregation of an impedance load and a PV plant.

Case A

The PV is generating 2 MW and the impedance load consumes 4 MW at nominal voltage. The aggregation thus consumes both active and reactive power in total. The nRMSE values comparing the ZIP currents to the reference current all lie below 0.03 and this confirms that the solved optimization has converged well.

We have seen in Table 5 – Powers absorbed by each branch of different symmetric ZIP models of the PV generating 1990 kW and absorbing 99.9 kVAr.

of Section 3.3.2 that the PV is mainly represented by I- and S-branches of the ZIP equivalent. So we expect that the ZIP Z- branches represent the impedance load at the MV level. As the load both consumes active and reactive power, we compare the identified values of R and L to the true equivalent MV impedance inferred by measuring the current contribution of the impedance load. Table 6 and

Table 7 show the results for the asymmetric and symmetric ZIP equivalents, respectively. The error in the estimation is at least 5%. We can see that the estimation gets better if the data used for the identification contains bigger voltage drops. It is especially true for the estimation of the resistance. However, the matching is not as accurate as for the identification of a pure impedance load (see Section 3.3.1).

Table 6 – Impedance matching for the identification of Aggregation A using asymmetric ZIP equivalents. The columns e_R and e_L show the relative errors.

		R [Ω]	L [H]	R_{zip} [Ω]	L_{zip} [H]	e_R [%]	e_L [%]
asymmetric ZIP 3 %	phase A	31.58	0.19	43.27	0.20	37.0	7.5
	phase B	31.58	0.19	28.57	0.22	9.5	15.7
	phase C	31.58	0.19	21.46	0.31	32.1	63.0
asymmetric ZIP 10 %	phase A	31.58	0.19	27.22	0.22	13.8	17.5
	phase B	31.58	0.19	23.38	0.22	26.0	15.5
	phase C	31.58	0.19	22.36	0.25	29.2	29.6
asymmetric ZIP 30 %	phase A	31.58	0.19	29.43	0.22	6.8	16.9
	phase B	31.58	0.19	28.52	0.22	9.7	16.6
	phase C	31.58	0.19	27.45	0.23	13.1	20.3

Table 7 – Impedance matching for the identification of Aggregation A using symmetric ZIP equivalents. The columns e_R and e_L show the relative errors.

	R [Ω]	L [H]	R_{zip} [Ω]	L_{zip} [H]	e_R [%]	e_L [%]
symmetric ZIP 3 %	31.58	0.19	20.38	0.23	35.5	20.4
symmetric ZIP 10 %	31.58	0.19	35.62	0.22	12.8	17.8
symmetric ZIP 30 %	31.58	0.19	29.72	0.23	5.9	19.2

For the fault simulations, the reference device and the asymmetric and symmetric ZIP equivalents are successively connected to the bus in the network close to the fault and the voltage and current waveforms are recorded. Table 8 shows the voltage drops occurring at the bus for the different devices. They are again very similar, which is very good and allows us to focus on the current matching.

Table 9 shows the values of the nRMSE when comparing the currents of the different ZIP models to the current drawn by the true device. We can observe a few things. First, the matching is really good for symmetric faults (nRMSE close to 0) for the case with 10Ω fault resistance, because the voltage drop is small. For ABC 1Ω faults, the asymmetrical ZIP model achieves a better matching. Similarly, to the identification of the single PV in Section 3.3.2 we can see that data with more significant voltage drops is needed to achieve a good matching with the symmetric ZIP model. The symmetric model has less degrees of freedom, which restrict its ability to adapt itself to each phase.

Second, the symmetric model mostly achieves a better matching for asymmetric faults. The matching is good for Ag faults with nRMSE values below 0.2. However, for 2-phase faults, the performance is only acceptable for the symmetric ZIP identified using a 30% voltage drop in the data. This is again due to the bigger voltage drops caused by the 2-phase faults. The symmetric ZIP performs better as it represents a PV plant more accurately during asymmetric faults (see Section 3.3.2).

Figure 18 and Figure 19 show the voltage and current matching during ABC 1Ω and ABg 1Ω faults respectively for the ZIP identifications using a 30% voltage drop in the data. It is clearly visible that the asymmetric ZIP model performs better during symmetric faults and that the symmetric ZIP model performs better during ABg faults. The maximal current error for the symmetric ZIP model is around 155 A for the ABC 1Ω fault and 110 A for the ABg 1Ω fault.

Table 8 – Voltage drops during faults for the simulations with different ZIP equivalents of Aggregation A.

	ABC		AB		ABg		Ag	
	1Ω	10Ω	1Ω	10Ω	1Ω	10Ω	1Ω	10Ω
reference	34 %	6 %	21 %/57 %	3 %/12 %	60 %	52 %	34 %	6 %
asymmetric ZIP 3%	34 %	6 %	21 %/57 %	3 %/12 %	60 %	52 %	34 %	6 %
symmetric ZIP 3%	34 %	6 %	21 %/57 %	3 %/12 %	60 %	52 %	34 %	6 %
asymmetric ZIP 10%	34 %	6 %	21 %/57 %	3 %/12 %	60 %	52 %	34 %	6 %
symmetric ZIP 10%	34 %	6 %	21 %/57 %	3 %/12 %	60 %	51 %	34 %	6 %
asymmetric ZIP 30%	34 %	6 %	21 %/57 %	3 %/12 %	60 %	52 %	34 %	6 %
symmetric ZIP 30%	34 %	6 %	21 %/57 %	3 %/12 %	60 %	52 %	34 %	6 %

Table 9 – nRMSE of the fault current absorbed by the identified ZIP models with respect to the reference of Aggregation A.

	ABC		AB		ABg		Ag	
	1Ω	10Ω	1Ω	10Ω	1Ω	10Ω	1Ω	10Ω
asymmetric ZIP 3%	0.27	0.05	0.46	0.05	0.63	0.68	0.17	0.02
symmetric ZIP 3%	0.48	0.05	0.67	0.07	0.68	0.66	0.17	0.02
asymmetric ZIP 10%	0.29	0.05	0.39	0.05	0.74	0.79	0.29	0.04
symmetric ZIP 10%	0.51	0.05	0.32	0.05	0.62	0.53	0.06	0.02
asymmetric ZIP 30%	0.15	0.05	0.42	0.06	0.64	0.70	0.22	0.04
symmetric ZIP 30%	0.30	0.05	0.19	0.05	0.18	0.16	0.06	0.01

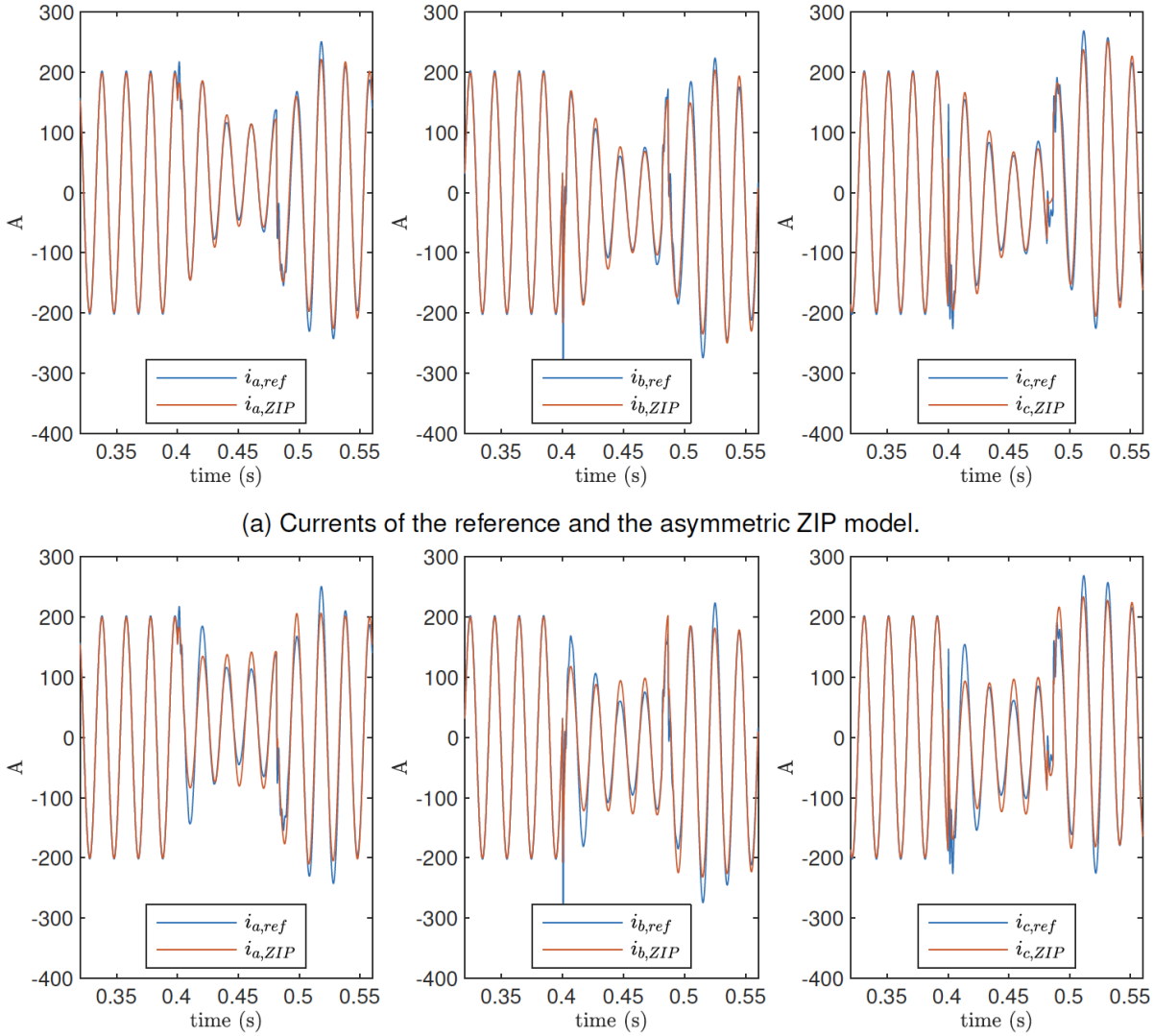

(a) Currents of the reference and the asymmetric ZIP model.

Figure 18 – Comparison for the ABC 1Ω fault using data with a 30% voltage drop to identify Aggregation A.

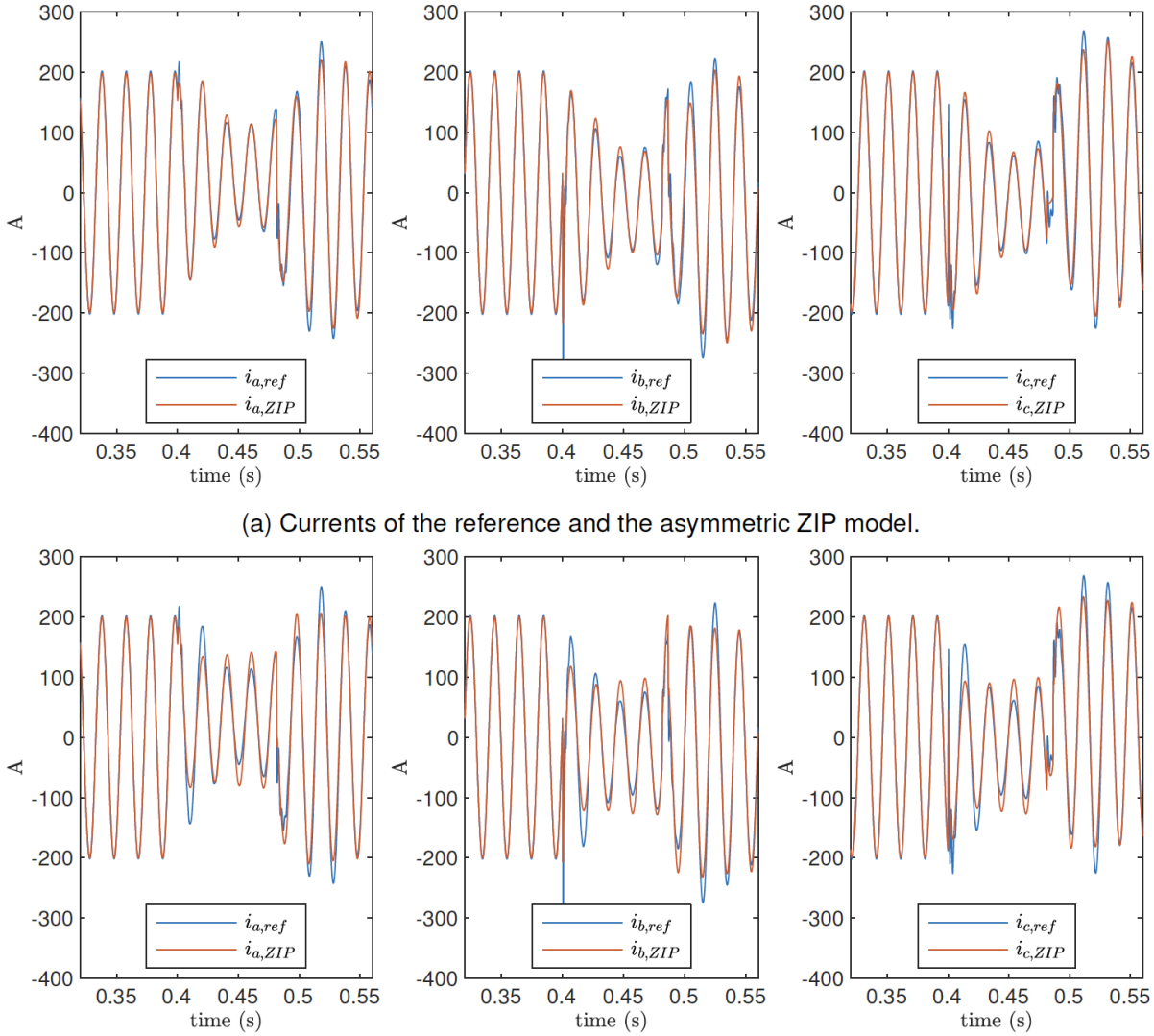

(a) Currents of the reference and the asymmetric ZIP model.

Figure 19 – Comparison for the ABg 1Ω fault using data with a 30% voltage drop to identify Aggregation A.

Case B

For this variant of the aggregation shown in Figure 17, the PV generates 8 MW and the load consumes 1 MW for nominal conditions. In total, the aggregation thus consumes reactive power but generates active power. We again identify both the asymmetric and symmetric ZIP models for the 3 data sets with 3 %, 10% and 30% voltage drops.

Table 10 and Table 11 show the identified values of R and L for the asymmetric respectively symmetric ZIP equivalents and compares them to the true impedance at the MV level. The values of the true impedance are estimated measuring the current of the impedance load at the MV level. For the data sets containing a 3% and 10% voltage drop, the estimation errors are very high. The impedance of the aggregation is not recognized. For the asymmetric ZIP model, the identifications of the 3 phases are independent. The impedance is not recognized and we get very different values among the three phases.

For the dataset containing a 30% voltage drop, the matching significantly improves and the symmetric ZIP model achieves the lowest errors. However, the error values still reach 40%.

Table 10 – Impedance matching for the identification of Aggregation B using asymmetric ZIP equivalents. The columns e_R and e_L show the relative errors.

	R [Ω]	L [H]	R_{zip} [Ω]	L_{zip} [H]	e_R [%]	e_L [%]
asymmetric ZIP 3 % phase A	126.4	0.76	1.002e+06	11599	792761	1531951
phase B	126.4	0.76	37.15	8341	71	1101611
phase C	126.4	0.76	15.12	955.4	88	126097
asymmetric ZIP 10 % phase A	126.4	0.76	1e+06	1.20	791078	58
phase B	126.4	0.76	17.08	15.66	87	1968
phase C	126.4	0.76	15.26	3.03	88	300
asymmetric ZIP 30 % phase A	126.4	0.76	414.7	0.85	228	11.6
phase B	126.4	0.76	43.36	1.51	65.7	98.8
phase C	126.4	0.76	33.84	0.98	73.2	29.9

Table 11 – Impedance matching for the identification of Aggregation B using symmetric ZIP equivalents. The columns eR and eL show the relative errors.

	R [Ω]	L [H]	R_{zip} [Ω]	L_{zip} [H]	e_R [%]	e_L [%]
symmetric ZIP 3 %	126.4	0.76	38.14	1.17	69.8	55.0
symmetric ZIP 10 %	126.4	0.76	4765	0.99	3670	30.1
symmetric ZIP 30 %	126.4	0.76	119.6	1.06	5.4	40.5

We perform the same fault simulations as before (described in Section 2.3.2), for the true aggregation and the identified ZIP models.

Table 12 shows the voltage drops occurring during the different faults, which are again very similar.

The values of the nRMSE when comparing the currents of the different ZIP models to the true current drawn by the aggregation are shown in

Table 13. We can observe the same trends we have already seen for the identification of the PV in Section 3.3.2 and aggregation A in Section 3.3.3. First, the asymmetric ZIP model achieves a better matching than the symmetric model for symmetric faults. For Aggregation B the performance is acceptable with errors below 0.25. Second, the symmetric model performs better for asymmetric faults because the PV is better represented using a symmetric model, as we observed in Section 3.3.2. Third, the performance of the symmetric ZIP equivalent during Ag faults is good already for the dataset with a 3% voltage drop only. The error for Ag faults lies below 0.1 for all symmetric ZIP identifications of Aggregation B.

The voltage drops in the faulty phases are highest for the 2-phase faults with a 1Ω fault resistance, which leads to higher nRMSE values. As for Aggregation A, the performance is only acceptable for the symmetric ZIP model using a 30% voltage drop in the identification data.

Table 12 – Voltage drops for the simulations with different ZIP equivalents of Aggregation B.

	ABC		AB		ABg		Ag	
	1Ω	10Ω	1Ω	10Ω	1Ω	10Ω	1Ω	10Ω
reference	31 %	2 %	18 %/56 %	-1 %/ 9 %	58 %	50 %	32 %	2 %
asymmetric ZIP 3%	31 %	2 %	16 %/56 %	-1 %/ 9 %	57 %	49 %	31 %	2 %
symmetric ZIP 3%	31 %	2 %	17 %/55 %	-0 %/ 9 %	57 %	49 %	32 %	2 %
asymmetric ZIP 10%	30 %	2 %	16 %/56 %	-1 %/ 9 %	57 %	48 %	30 %	2 %
symmetric ZIP 10%	30 %	2 %	17 %/56 %	-1 %/ 9 %	57 %	48 %	32 %	2 %
asymmetric ZIP 30%	31 %	2 %	17 %/56 %	-1 %/ 9 %	57 %	49 %	31 %	2 %
symmetric ZIP 30%	31 %	2 %	18 %/56 %	0 %/ 9 %	58 %	50 %	32 %	2 %

Table 13 – nRMSE of the fault current absorbed by the identified ZIP models with respect to the reference of Aggregation B.

	ABC		AB		ABg		Ag	
	1Ω	10Ω	1Ω	10Ω	1Ω	10Ω	1Ω	10Ω
asymmetric ZIP 3%	0.18	0.06	0.45	0.09	0.92	0.96	0.38	0.08
symmetric ZIP 3%	0.43	0.06	0.33	0.07	0.81	0.74	0.09	0.02
asymmetric ZIP 10%	0.25	0.06	0.47	0.09	1.36	1.30	0.51	0.08
symmetric ZIP 10%	0.44	0.07	0.27	0.07	0.77	0.68	0.07	0.02
asymmetric ZIP 30%	0.14	0.06	0.44	0.10	1.00	1.02	0.37	0.07
symmetric ZIP 30%	0.26	0.07	0.15	0.07	0.22	0.19	0.08	0.02

Despite the misestimation of the impedance, the performance of the ZIP equivalents is very good for symmetric faults (when using the asymmetrical model) and for Ag faults (when using the symmetric ZIP equivalents). The behaviour is dominated by the PV, which, at nominal voltage, generates eight times more power than the impedance load is consuming. Figure 20 and Figure 21 show the voltage and current matching during ABC and ABg faults respectively, for a fault resistance of 1Ω and using the dataset with a 30% voltage drop to identify the ZIP models. Apart from extremely quick spikes at the

fault inception, the maximal absolute current error is about 259 A during the ABC fault and about 283 A during the ABg fault for the symmetric ZIP model.

We have seen identifications of two different aggregations. Case A with a dominating impedance load and Case B with a dominating generation of active power. For case A, the impedance load is important enough such that it is well identified by the ZIP models. In Case B the impedance is not recognized. However, the amount of generated power is already quite big for a distribution system. It would be reasonable to connect the PV to a separate busbar and equip it with separate measurements. In that case, the PV and impedance load could be identified in separate procedures and we could expect a performance similar to the ones presented in Sections 3.3.1 and 3.3.2. For both aggregations, the presence of the PV always generating symmetric currents leads to the result that symmetric ZIP models perform better during asymmetric faults.

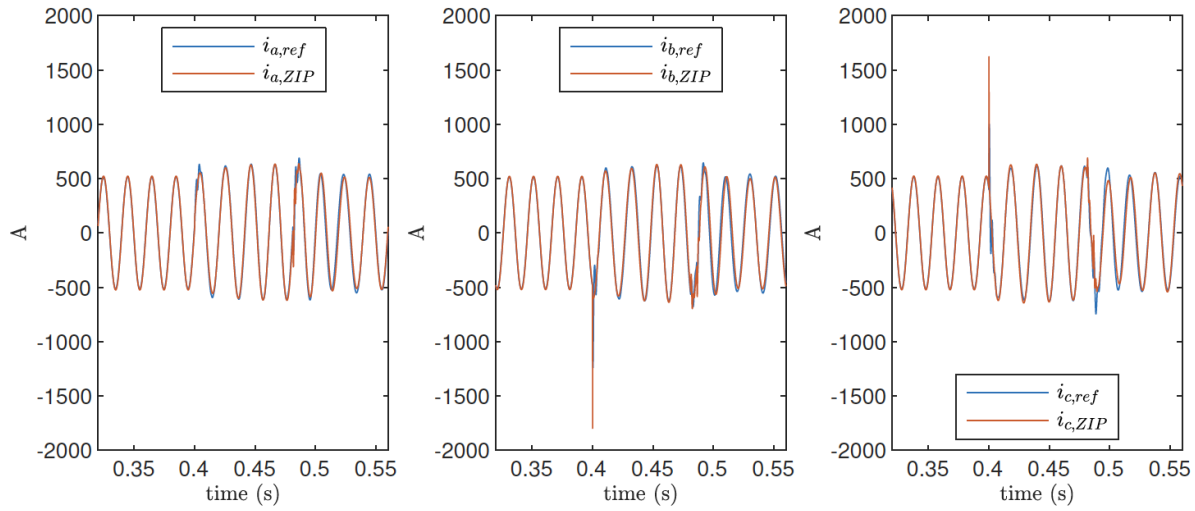

(a) Currents of the reference and the asymmetric ZIP model.

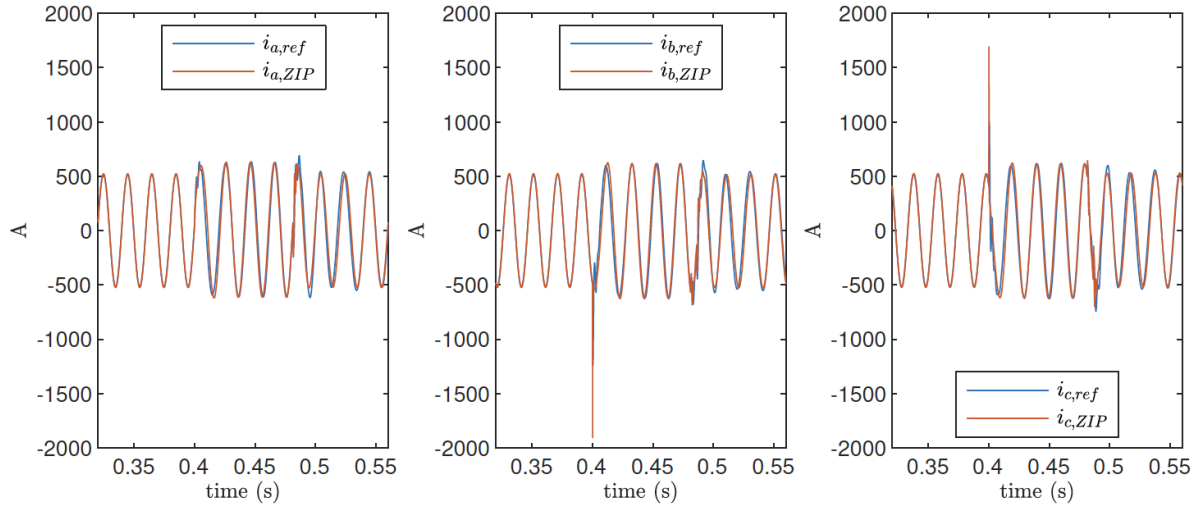

(b) Currents of the reference and the symmetric ZIP model.

Figure 20 – Comparison for the ABC 1Ω fault using data with a 30% voltage drop to identify Aggregation B.

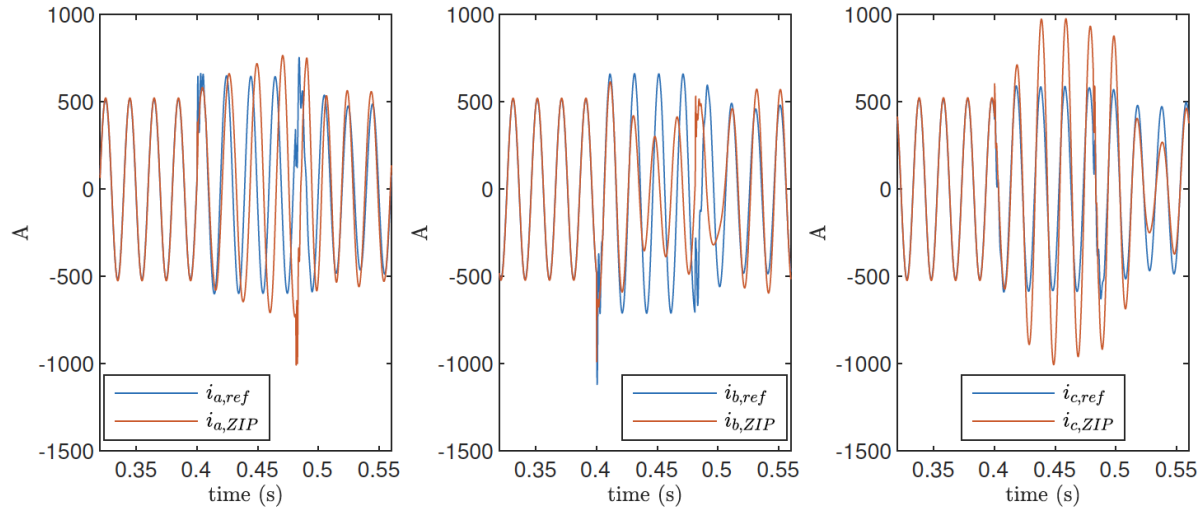

(a) Currents of the reference and the asymmetric ZIP model.

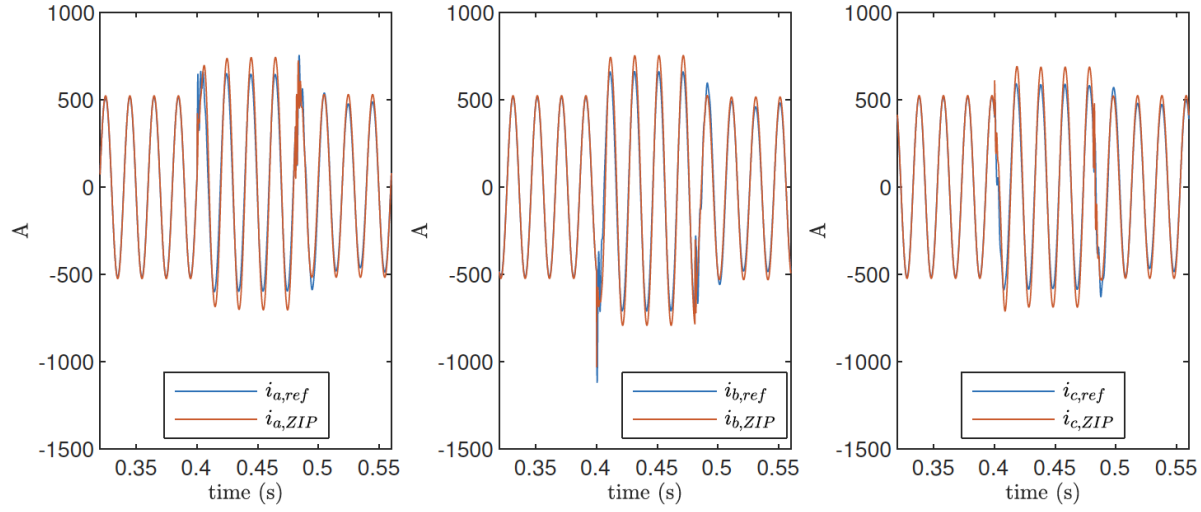

(b) Currents of the reference and the symmetric ZIP model

Figure 21 – Comparison for the ABg 1Ω fault using data with a 30% voltage drop to identify Aggregation B.

3.3.4 Remarks on the ZIP model identification results

We have presented the ZIP identification for three different types of loads using data containing different voltage steps. A pure impedance load and a PV plant were considered, which represent frequent elements in distribution systems, as well as aggregations of loads and generations.

For a load composed of a pure impedance, our procedure can precisely match the Z-branch of the ZIP with the true impedance of the node. Our procedure can also identify the impedance of an aggregation if its power consumption is large enough with respect to the total power measured at the node the aggregation is connected to.

Furthermore, a single device can be represented very well during symmetric faults by a ZIP equivalent identified using data containing voltage steps of only a few percent. We have verified the current matching of identified ZIP equivalents with respect to the reference device for the PV plant and for typical symmetric faults in the grid, which lead to voltage drops of around 35 %.

Finally, we have seen that the symmetric ZIP equivalent is much better suited than the asymmetric ZIP model to represent a PV plant (connected to the grid via a DC/AC converter) during asymmetric faults. We achieve a good matching (nRMSE ≤ 0.25) when using identification data containing a 30% voltage drop. The user can thus choose the appropriate ZIP model, asymmetric or symmetric, to represent a grid node depending on the desired short-circuit analysis and whether or not a generation is connected to the grid through an inverter.

3.4 Short-circuit analysis using ZIP equivalents

In this section we analyse the short-circuit currents in the medium-voltage grid of Veyrier operated by SIG. This grid was already the reference grid for the studies of the Working Package WP1 of the SynchroFAP project. To validate the proposed method for fault-current calculations, we use an EMTP-RV grid model where loads and generators are either modelled using reference models (the same used in section 2.2.5, namely an impedance for the loads and a very detailed PV model for the PV plant already provided in EMTP-RV) or using symmetric and asymmetric ZIP models.

We are interested in comparing the short-circuit currents at the nodes and especially at the MV infeed. The current amplitudes at this location are very important for tuning the protection devices, which are usually placed at the root of radial feeders. The following four different grids are considered:

- reference grid with the real loads and generations
- grid where asymmetric ZIP equivalents are used to represent the loads and generations
- grid where symmetric ZIP equivalents are used to represent the loads and generations
- reference grid without distributed generation

The last case will be called “passive grid”. It represents the grid model usually adopted for current short-circuit analyses in distribution grids, as distributed generation is seldom considered. Indeed, often distributed generation is unknown or is disconnected during faults. However, due to the increasing amount of DG in distribution grids, the European Network Transmission Systems Operator (ENTSO-E) has recently established a common framework [3] to avoid DG disconnection during a fault, with the aim of guaranteeing the power balance of the system. This requirement for DG, referred to as Fault Ride Though (FRT) capability, is nowadays always specified in detail in the grid codes.

The following sections present the configuration of the reference grid, the results of the ZIP identification and current comparisons and finally an example of the use of ZIP models in short-circuit analyses. The motor convention is again used for the power specifications.

3.4.1 Reference grid

The network chosen as a reference is shown in Figure 22. It has an under-compensated neutral tuned to reach fault current amplitudes of 50 A for solid phase-to-ground faults. The nominal RMS value of the MV line-to-line voltage is 18.2 kV. Two PV plants generate 8 MW each and are connected close to the MV infeed. As in Section 3.3.2, they generally do not disconnect themselves from the grid for the simulated short-duration faults. The remaining load buses have impedance loads connected via Dy transformers, with nominal power consumption as shown in Table 14.

Table 14 – Impedance loads of the reference grid.

	P_{3ph} [kW]	$cos(\phi)$	V_{LV} [kV]	$S^n_{transformer}$ [kVA]	V_{MV} [kV]
L_1	300	0.9	0.42	1250	18.2
L_2	90	0.9	0.42	630	18.2
L_3	30	0.9	0.985	250	18.2

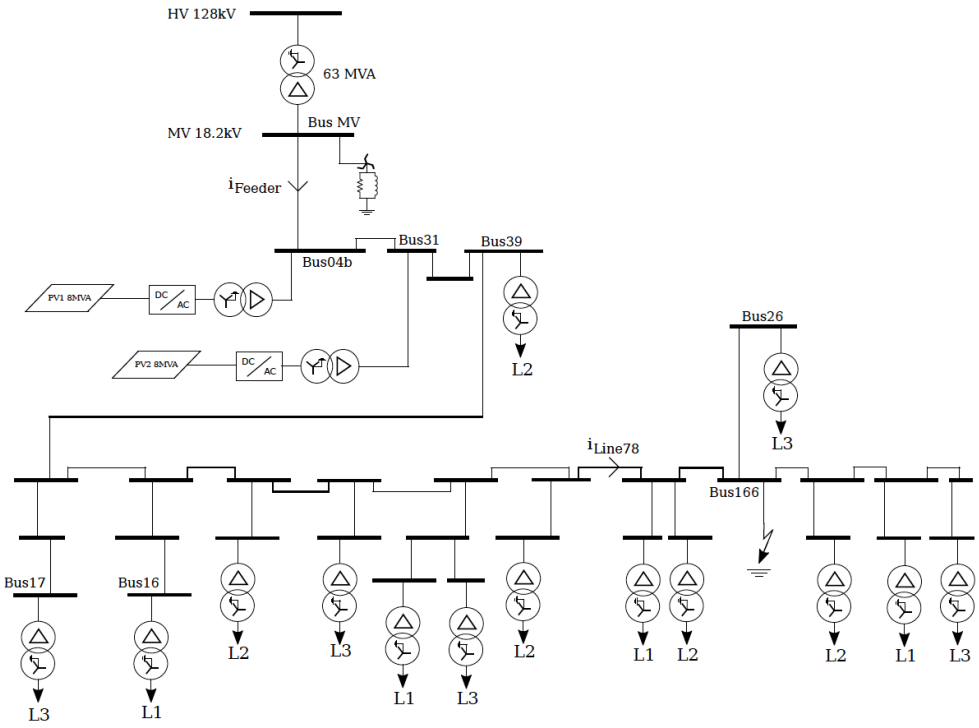

Figure 22 – Reference grid.

3.4.2 ZIP equivalents

The grid with only ZIP equivalents at the different nodes is represented in Figure 23. We used a voltage drop of around 10% in the MV network to perform the ZIP identifications of the PV and the three load types. The voltage step was generated simulating the connection of a big load to the HV grid and the voltage and currents waveforms at the nodes were recorded for 200 ms before and after the step. The data at nodes B04b, B16, B39 and B17 are used to identify the PV and loads L1, L2, L3. The four devices (the PV and the three impedance loads) were identified using asymmetric and symmetric ZIP model. Finally, we obtain a grid where all the loads and generators are represented by symmetric ZIP models and another grid with asymmetric ZIP models.

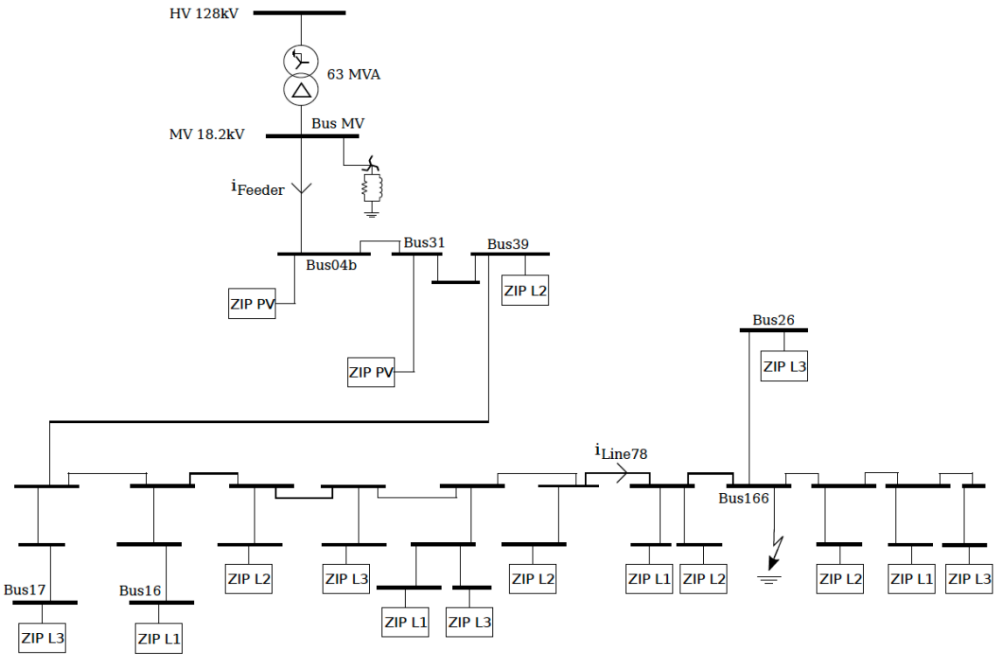

Figure 23 – Grid with ZIP equivalents.

3.4.3 Comparison of short-circuit currents

The currents in the different grids are compared for faults occurring downstream of the PV nodes at bus 166 shown in Figure 17. The same fault types are used as in Section 2.3.2 (see Figure 3) and R_f is set to 1Ω or 10Ω. We compare the voltage drops occurring in the different grids and the currents injected to the nodes by the reference devices and the ZIP equivalents. The nRMSE metric described in Eq. (3) is used to evaluate the current matching.

PV nodes

Table 15 shows the nRMSE of the different node currents with respect to the reference case, averaged over the faulty phases. One row shows the values of nRMSE(i_{ref} ,$\hat{\imath}$) for the different fault simulations, where $\hat{\imath}$ refers to the node current from the grids with asymmetric or symmetric ZIP equivalents or to the currents from the passive grid. Only the samples during the fault are used to evaluate the errors.

We can see that the error stays below 0.09 for the representation with symmetric ZIP, which is a really good matching. For the grid using asymmetric ZIP models, the matching worsens significantly for asymmetric faults. We have seen in Section 3.3.2 that the PV is only well represented during asymmetric

faults when using the symmetric ZIP equivalent. Both the true PV plant and the symmetric ZIP model always generates symmetrical currents.

As there is no current injection at the considered nodes for the passive grid, the nRMSE values equal 1 for all fault simulations for this grid configuration.

Table 15 – nRMSE of the fault current absorbed at nodes B04b and B31 by the identified ZIP models with respect to the reference case.

	ABC		AB		ABg		Ag	
	1Ω	10Ω	1Ω	10Ω	1Ω	10Ω	1Ω	10Ω
B04b asymmetric ZIP	0.06	0.04	0.05	0.05	0.45	0.43	7.52	2.58
B04b symmetric ZIP	0.08	0.04	0.05	0.04	0.05	0.05	0.02	0.02
B31 asymmetric ZIP	0.06	0.04	0.05	0.04	0.44	0.43	5.40	2.35
B31 symmetric ZIP	0.08	0.04	0.05	0.04	0.05	0.05	0.02	0.02

Currents at the root of the MV feeder and in line 78

We compare the currents at the root of the MV feeder (Bus MV) and in line 78, as they represent very different parts of a MV grid. Line 78 is located downstream the PVs (see Figure 22). During faulty conditions, the currents in line 78 are thus fed by the PV plants and the grid upstream. This leads to the so-called blinding effect [9] for the protection placed at the root of the feeder, which means that the fault current measured by the protection relay at the root of the feeder is lower than the fault current flowing in the feeder downstream, due to the additional short-circuit current contribution of the PV plant placed between the relay and the fault. Therefore, being the relay tripping time too high due to the blinding effect, line 78 can be seriously damaged.

Table 16 shows the nRMSE values of the current at the root of the feeder (node MV) and in Line 78 for the three grid types (grid with asymmetric ZIP models, grid with symmetric ZIP models or the passive grid), considering multiple fault scenarios.

Overall, the grid with the symmetric ZIP representations of the nodes achieves the best performance with errors below 0.05. If we consider symmetrical faults only, the asymmetric ZIP models yield slightly better matching. For asymmetrical faults, only the symmetric ZIP models perform well. The passive grid performs poorly when comparing the short-circuit currents at the root of the MV feeder as it ignores the significant fault current contribution of the PV. For the passive grid, the highest error occurs for single phase-to-ground faults. In that case, the fault current has the lowest value and the missing relative contribution of the PV to the total fault current has a higher impact compared to the other cases.

Table 16 – nRMSE of the fault currents at node MV (root of the MV feeder) and in line 78 for the different grid configurations with respect to the reference case.

	ABC		AB		ABg		Ag	
	1Ω	10Ω	1Ω	10Ω	1Ω	10Ω	1Ω	10Ω
Bus MV asymmetric ZIP	0.01	0.04	0.01	0.02	0.06	0.06	7.72	2.93
Bus MV symmetric ZIP	0.01	0.05	0.01	0.02	0.01	0.01	0.02	0.02
Bus MV passive grid	0.18	1.14	0.18	0.53	0.15	0.15	1.21	1.21
Line78 asymmetric ZIP	0.00	0.00	0.00	0.00	0.02	0.02	0.54	0.36
Line78 symmetric ZIP	0.00	0.00	0.00	0.00	0.00	0.00	0.00	0.00
Line78 passive grid	0.03	0.03	0.03	0.03	0.03	0.03	0.03	0.03

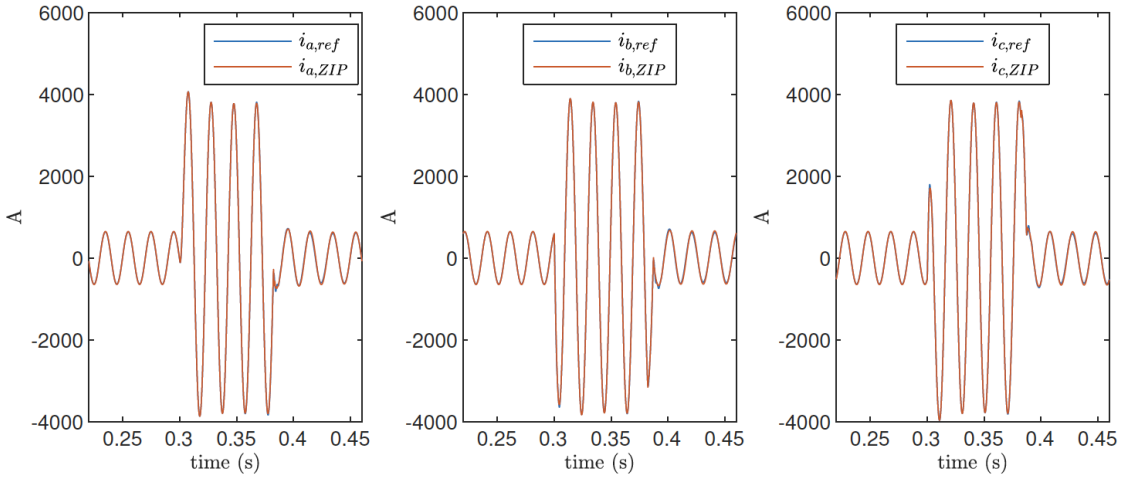

(a) Currents of the reference and the asymmetric ZIP model.

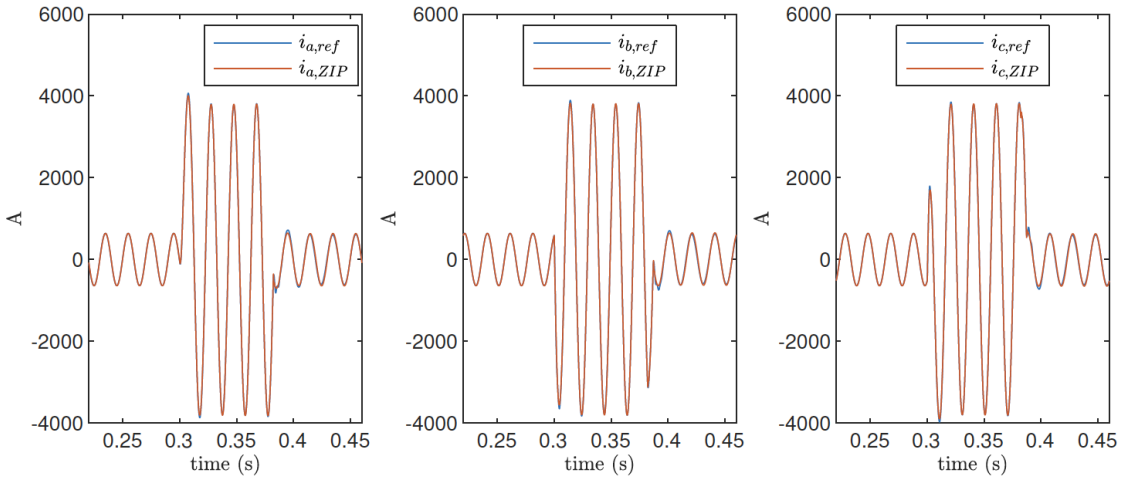

(b) Currents of the reference and the symmetric ZIP model.

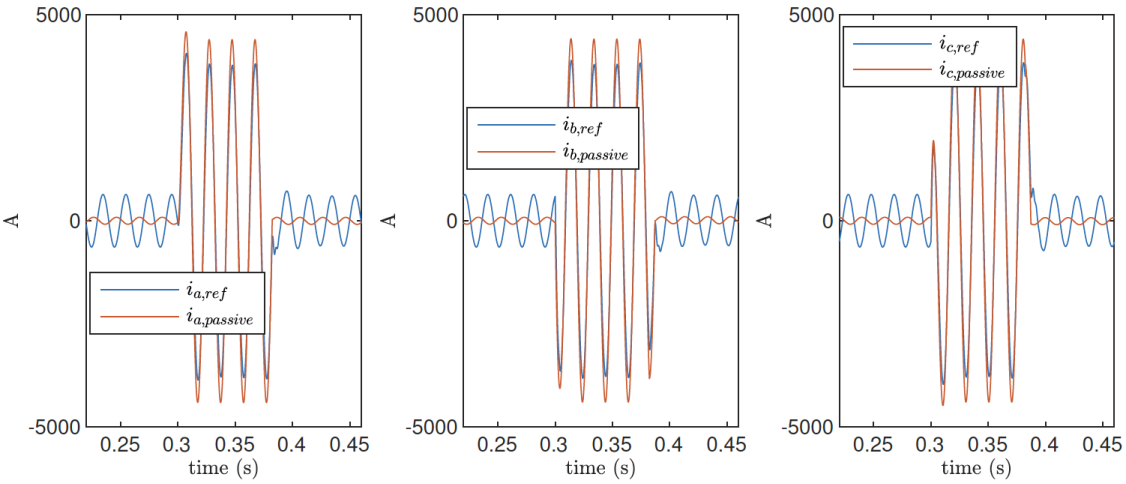

(c) Currents of the reference and the passive grid.

Figure 24 – Comparison at the root of the MV feeder for the ABC 1Ω fault.

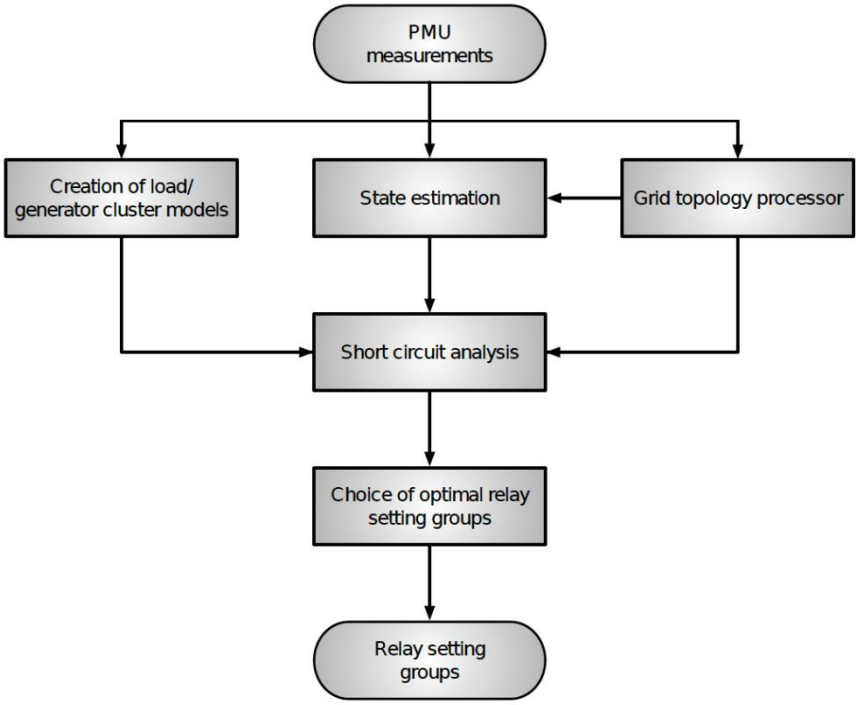

Figure 25 – Adaptive protection algorithm.

3.5 Adaptation of protection settings

In this section we have demonstrated that we are able to correctly estimate the short-circuit currents in a grid by accurately modeling the dynamic response to faults of loads and generators. In this way, we can identify the possible dangerous situation that were illustrated in Section 3.1 The outcome of that was that the main threaten for the proper functioning of the protection system was the blinding effect of the overcurrent relay placed at the root of the feeder. This phenomenon typically occurs when there is a 3-phase or 2-phase fault with fault resistance of a few ohms.

At this point, we need to adapt the settings of the protection relays, which is the last stage depicted in Figure 25. The adaptation of the protection settings to avoid the blinding is quite straightforward: as soon as the short-circuit analysis points out the presence of the blinding effect, the values of the instantaneous overcurrent threshold should be decreased. The recommendation made in Section 3.1 was to lower the threshold to 800 A for the protection at the root of the feeder, when the generation increases to 12 MW, or also to set an additional fixed delayed threshold.

The last activities we realized consisted in the implementation in a real-time simulation environment of the switching between various setting groups of a relay when a blinding threaten is identified. A technical demonstration was performed at the end of the project and whose setup is described in Section 3.6.

3.6 Technical demonstration

The study has been validated using a real-time Hardware-In-the Loop (HIL) simulation environment allowing the interaction between simulated quantities (e.g., the model of the grid and the synchrophasor extraction algorithm) with actual physical devices namely a signal amplifier, a protective relay and a Phasor Data Concentrator (PDC). The interface between simulated and real quantities is obtained by means of either analog signals or digital signal transmitted over commercially available protocols.

Accurate grid modeling in a real-time computation environment, associated to real components from the market, allows to reproduce the behavior of a given electrical network and validate the protection schemes under test in steady-state, dynamic and faulted conditions.

The setup of the demonstrator is schematically resumed in Figure 26, in which the solid arrows represent the traditional wired connection to transfer analog/digital signals between the OPAL-RT real-time simulator (RTS) and the ABB REF 615 protection relay [10] through an OMICRON CMS 356 amplifier. The dashed arrows represent data flows of PMU measurements based on IEEE C37.118 protocol, and the relay setting groups transmitted via the IEC-61850 protocol.

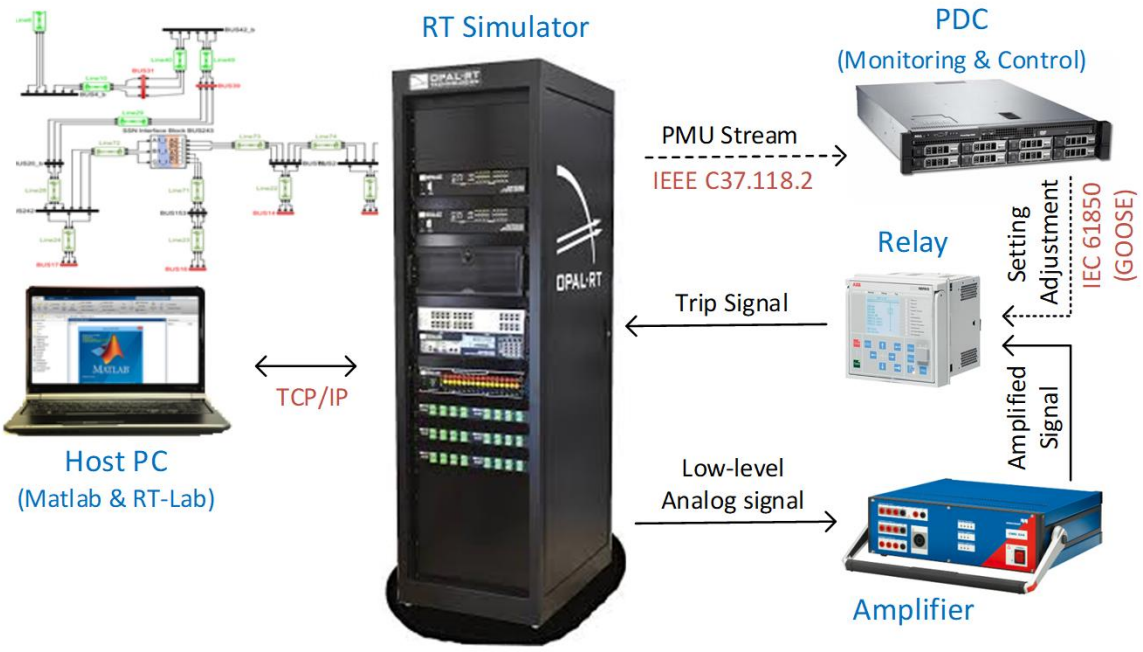

Figure 26 – HIL PMU-based adaptive protection scheme

The model of the grid described in Section 2.1 has been implemented in RT-LAB, the MATLAB-Simulink-based environment adopted by the OPAL-RT simulator, as shown in Figure 27. It is worth mentioning that the most appropriate simulation environment has been chosen in each phase of the project, namely, EMTP-RV for efficient time-domain short-circuit analysis and RT-LAB for real-time HIL validation.

As illustrated in Figure 26, the PDC included in the Zaphiro SynchroHub controller receives the synchrophasor measurements associated to the currents injected by the distributed generation modelled in the RT Simulator. This information is then used to select the most appropriate setting group on the relay (by sending a GOOSE message to the relay) from a table containing pre-calculated ones. At the same time, the protection relay receives fault current inputs from the RT Simulator (through a current amplifier) and, based on the setting determined by the SynchroHub, decides to clear a fault by sending a tripping signal to the RT Simulator to open the circuit breaker. The protection relay used here is an ABB REF615.

The key components of the setup are described as follows:

OPAL-RT Real Time Simulator

Opal-RT simulator consists of hardware and software components. On the software part, RT-LAB is fully integrated with MATLAB/Simulink environment, widely used within both academia and industry. In order to enable Simulink model to interact with the real world in real time through Opal-RT, we followed RT-LAB modeling rules by running the simulation in a multi-core real time operating system environment. Once the model is built and compiled in Simulink, it is deployed and runs into the Opal-RT hardware. RT-LAB handles synchronization and real-world interfacing using digital and analog I/O boards and TCP/IP or UPD data streams. For transmission and reception of synchrophasor streams, we leveraged on the IEEE C37.118 protocol. When used in slave (send) mode, the RT-LAB driver allows to stream synchrophasors' data from the simulator to Zaphiro's SynchroHub or any other IEEE C37.118 compliant devices. It is important to remark the PMUs modeled inside of the RTS are characterized by the same IEEE-compliant synchrophasors extraction algorithm available in the devices commercialized by Zaphiro. For details about implementation, characterization and experimental validation of the PMU algorithm into the RTS refer to [11].

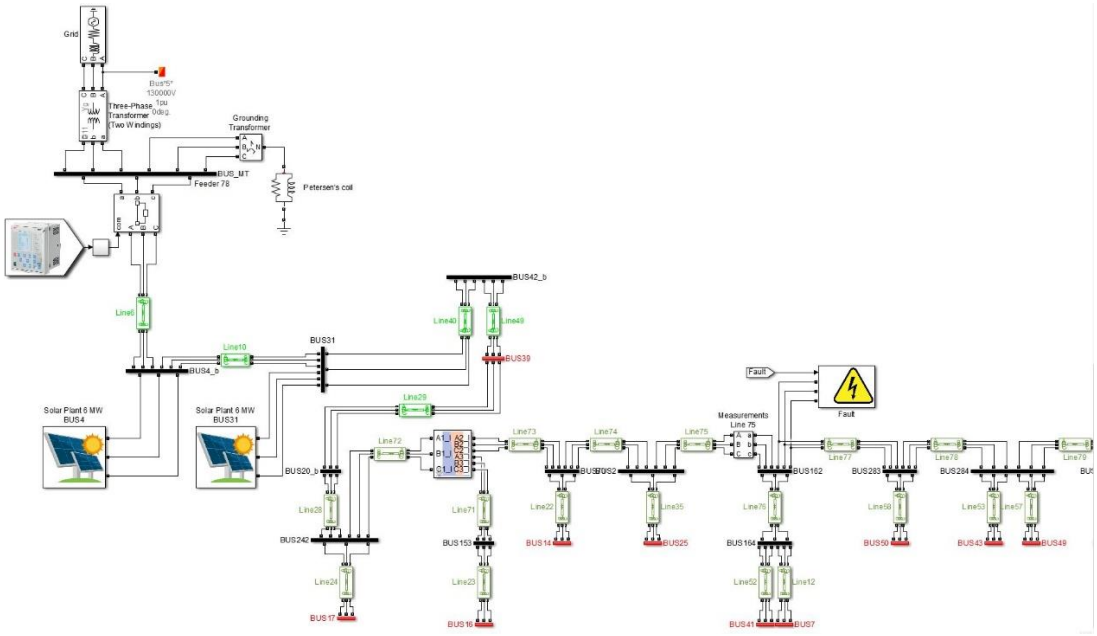

Figure 27 – RT-LAB model of feeder F78 of the MV grid of SIG

SynchroHub

SynchroHub is the Zaphiro's PDC. Its goal is to collect and process the data of the PMUs. It is qualified as a smart PDC since it is not just collecting data. Its software modules enable several power-system related functionalities (e.g., real-time state estimation, fault location). For this study, a module able to detect and communicate to the relay REF615 the proper setting group to use was developed.

REF615

REF615 is a dedicated relay for protection, control and supervision of distribution feeders, including radial and meshed distribution networks, with or without distributed power generation. It supports the IEC 61850 protocol, and several setting groups can be defined on it. It can receive both analog and digital input and can as well send digital signal to other devices such as circuit breakers or other relays.

The ABB dedicated software PCM 600 allows the operator to create logical connections between inputs of the relay and outputs. Several “common” protections functions are implemented directly in the REF615 and can be tuned depending on the need of each specific situation.

Power amplifier
An OMICRON CMS 356 current amplifier has been used to adapt the 10V analog output waveform of the Opal-RT into a 5A input the REF615.

The validation of the proposed adaptive protection scheme using an HIL approach can be summarized as follows:

a) The SIG sample network is modeled in Simulink using the power system toolbox.

b) The model is compiled and loaded into the OPAL-RT hardware.

c) Based on the level of the injected power by PVs, two setting groups are defined in the REF615 relay.

d) The currents flowing in the circuit breaker in the beginning of the feeder are sent from the analog outputs of the OPAL-RT module to the REF615 through the Omicron amplifier.

e) Two simulated PMUs transfer the synchrophasor measurements of voltage and currents at the PV locations to the SynchroHub using the C37.118 drivers of the OPAL-RT.

f) Synchrohub chooses the proper setting group for REF615 based on the measured level of PV power (adaptive protection).

g) Using one of the OPAL-RT digital inputs, the trip signal of the REF615 relay is acquired and used to trip the circuit breaker modeled at the beginning of the feeder.

Description of the technical demonstration
The technical demonstration was performed at the EPFL and made available by online streaming to all the participants. Some actual screenshots of the pc hosting the demo are presented in this section.

The portion of the MV grid modeled into the RT simulator is the same F78 feeder presented in Section 3.1. Two levels of PV generation are considered: low (6 MW) and high (12 MW).

The demo was articulated in three scenarios:

- Scenario 1 - Fault occurring while generation is low → relay trips normally
- Scenario 2 - Fault occurring while generation is high → relay does not trip because of blinding
- Scenario 3 - Fault occurring while generation is high and threshold has been adapted → relay trips because not affected by blinding anymore

The same symmetrical fault is simulated at the end of the feeder for the three scenarios.

Scenario 1

6 MW of photovoltaic generation are injected into the line and the threshold of the overcurrent relay is set to 1kA (defined as setting group 1). Once the fault is triggered in the RT simulator, a current of 1.4 kA flows at the fault location, 250 A of which come from the PV power plant. The relay senses then a current of about 1.2 kA and trips instantaneously, as illustrated in Figure 28.

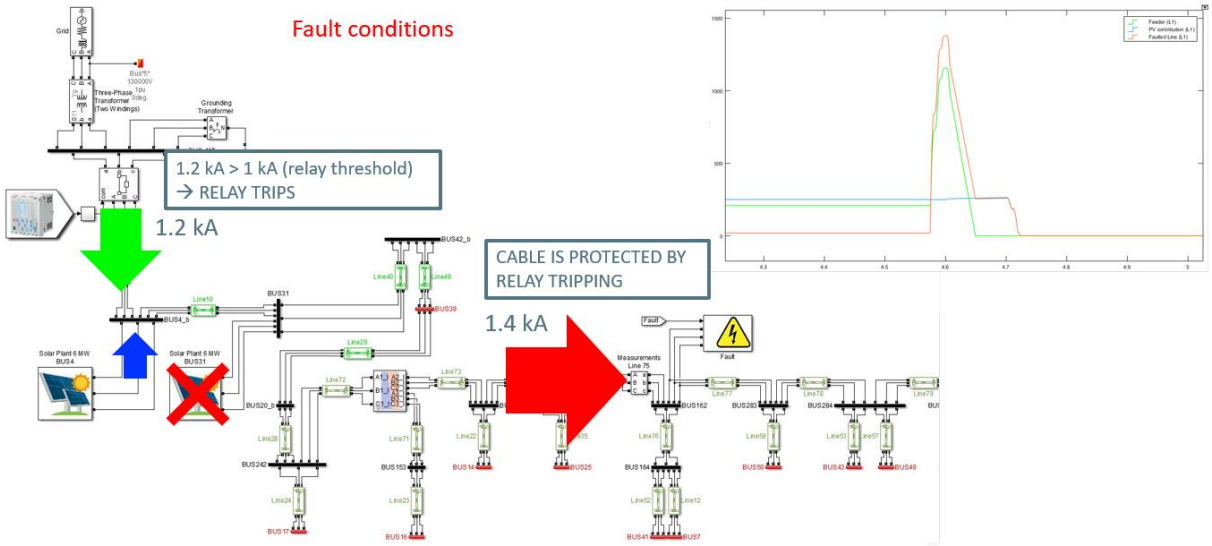

Figure 28 – Fault simulation for Scenario 1

Scenario 2

12 MW of photovoltaic generation are now injected into the line while the threshold of the overcurrent relay is still set to 1kA (defined as setting group 1). Once the fault is triggered in the RT simulator, a current of 1.4 kA flows at the fault location, around 500 A of which come now from the PV power plant. The relay senses then a current of around 900 A, lower than the instantaneous overcurrent threshold. Therefore, the relay does not trip because of the blinding effect produced by the high contribution to the fault current coming from the distributed generation. The screenshot presented in Figure 29 includes a photo of the relay that measures 912 A and does not trip.

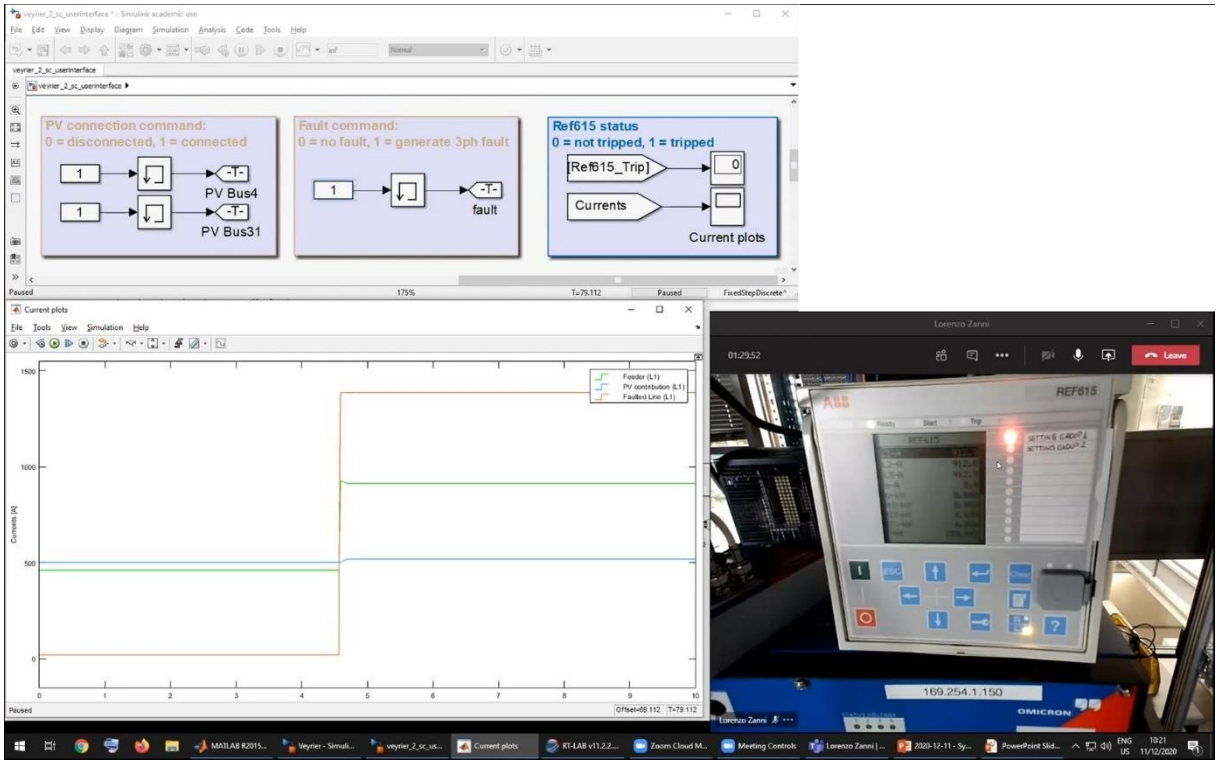

Figure 29 – Fault simulation for Scenario 2

Scenario 3

In this third scenario, the generation increases suddenly from 6 MW to 12 MW to show that the SynchroHub reacts by modifying on the fly the setting group of the relay (the setting group 2 is selected as illustrated in Figure 30).

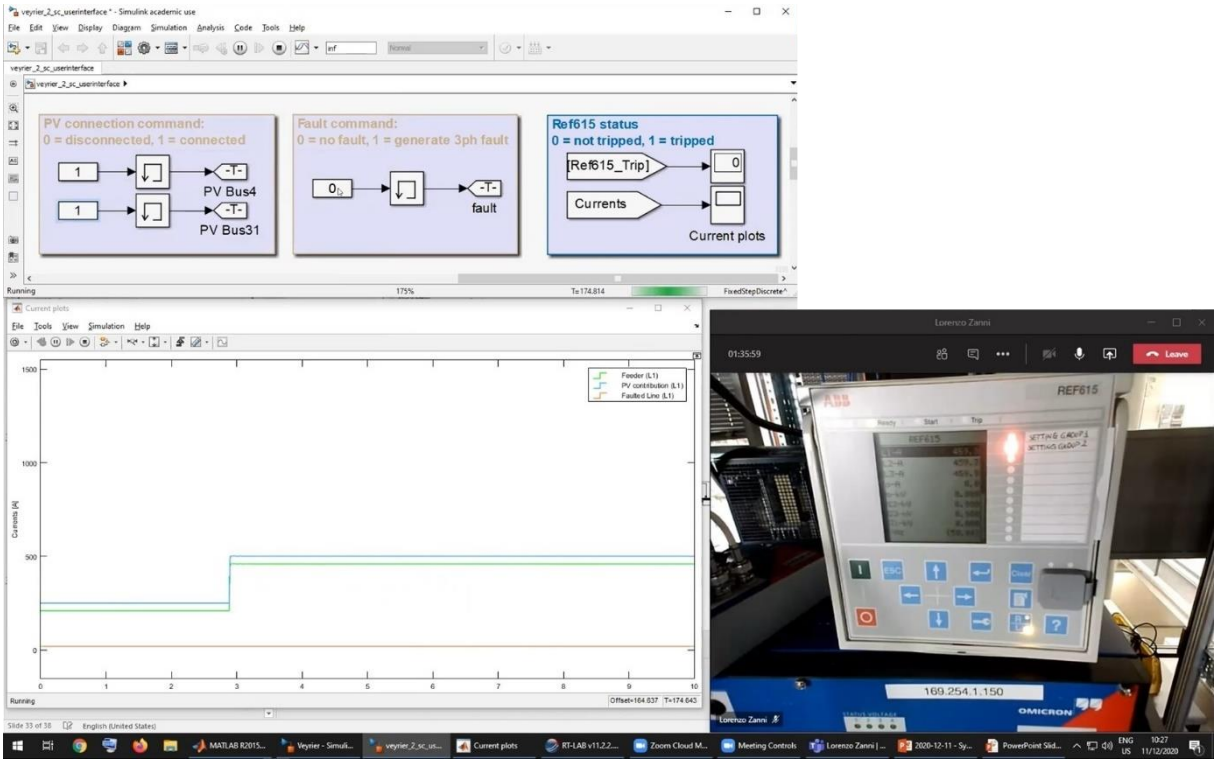

Figure 30 – Setting group modified by the SynchroHub as soon as a risk of blinding is detected

A fault is then produced at the end of the feeder, resulting in the same current values characterizing the Scenario 2, namely 1.4 kA for the fault current and around 500 A coming from the PV generation. Since this time the threshold has been decreased to less than 900 A, the same fault that was missed in the Scenario 2 is now correctly detected and the relay trips instantaneously, as shown in Figure 31. As soon as the fault is cleared, the setting group goes back to the default one (setting group 1).

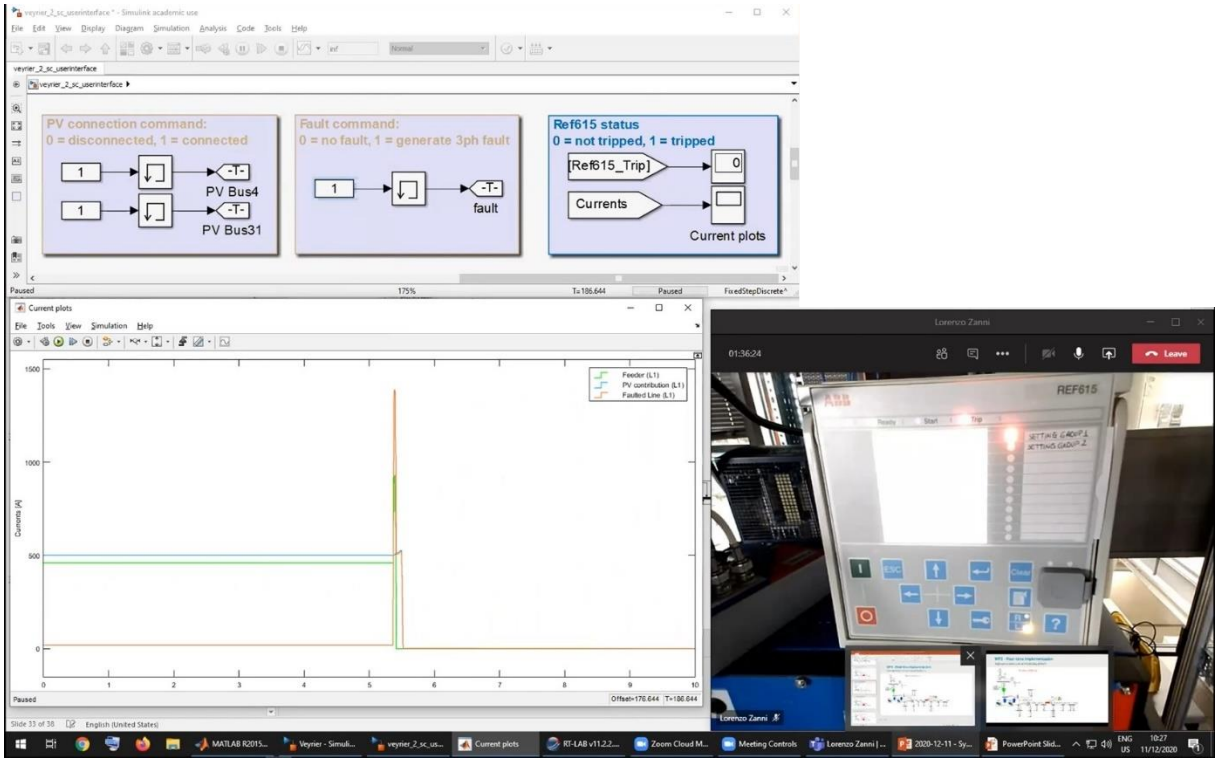

Figure 31 – After adaptation of its threshold, the relay detects correctly the fault

4 Conclusions

Significant portions of the MV network of the SIG were modeled to assess the performances of its protection scheme against an important increase of PV production according to the objectives of the Canton of Geneva for the horizon 2030.

The reliability of the protection scheme has been tested systematically for both symmetrical and asymmetrical faults, for various grid topologies and fault locations, as well as adopting different values of short-circuit impedance.

Regarding severe faults (three-phase faults and phase-to-phase faults), some occurrences of *blinding* were found when increasing the level of DG towards the quantities expected in the future, while no occurrences of *sympathetic tripping* were found under the same circumstances. New settings of the overcurrent relays have been proposed to eliminate the occurrence of blinding in case of high share of DG in service.

The performances of the protection scheme have been assessed against phase-to-ground faults as well, revealing no impact of the increasing share of DG due to the absence of zero-sequence components in their connection.

Some vulnerabilities of the present settings have been highlighted, namely, in case of high-impedance ground faults or when the Petersen coil is for some reasons disconnected. The fault detection can be improved by adopting a different algorithm for directional earth-fault protection, as proposed.

Modeling load/generation clusters like ZIP equivalents appears to be an innovative elegant solution to solve the problem of the unpredictability of their behaviour during short-circuits. Nevertheless, the tuning of the ZIP model appears to be too expensive in computational time to be performed in real time, so that the short-circuit analysis can only be performed offline. Further research efforts are needed to solve this limitation. It must be said that, even from the hardware point of view, the protection relays available on the market do not allow to change their settings in real time but only to select among predefined setting groups, which can be acceptable in a first time. Further discussions are needed with the relays' manufacturers to see whether this feature might be considered in their future developments.

The technical feasibility of implementing the proposed scheme into existing protection infrastructure has been proven by a technical demo, featuring actual PMUs and protection relays.

5 Outlook and next steps

The DSO involved in this study, namely, Services Industriels de Genève (SIG), wishes to install a pilot system implementing the described adaptive protection scheme on a selected feeder of its MV grid. The pilot system will be kept running in parallel to the existing protection system to provide ground-proof assessment of its performances and to gain experience in its exploitation. It has to be noticed that the present level of installed PV capacity is not yet important enough to justify the use of the described adaptive scheme. Its adoption will be needed in some years, depending how quick the target of 350 MW of installed capacity will be met.

Discussion are ongoing among the project partners and SIG to submit a proposal to SFOE for a P+D project in this direction, expected in 2021.

6 National and international cooperation

A DSO in the Netherlands has expressed interest in the developed approach and is currently discussing with Zaphiro Technologies about the practical applicability of the adaptive scheme in a typical MV grid.

7 Publications

The results of the investigations carried out throughout the SynchroFAP project have made the object of two publications:

- B. Vogel, *Distribution d'électricité: un disjoncteur pour tous les cas* (German version: *Eine Sicherung für alle Fälle*), Swiss Engineering RTS, March 2021.
- D. Pavanello, L. Zanni, *Un réseau électrique qui s'adapte au soleil*, Bulletin.ch Electrosuisse, 5/2021.

8 References

[1] Working Group C4.605, "Modelling and Aggregation of Loads in Flexible Power Networks", February 2014.

[2] T. A. Short, "Electric Power Distribution Handbook", Chapter 8, 2nd edition, CRC Press, May 19, 2014.

[3] European Network of Transmission System Operators for Electricity (ENTSO-E), "Draft Network Code on Demand Connection", December 5, 2012.

[4] L. V. Strezoski and M. D. Prica, \Short-circuit analysis in large-scale distribution systems with high penetration of distributed generators", IEEE/CAA Journal of Automatica Sinica, vol. 4, no. 2, pp. 243-251, April 2017.

[5] J. Mahseredjian, S. Denneti_ere, L. Dub_e, B. Khodabakhchian and L. G_erin-Lajoie, "On a new approach for the simulation of transients in power systems", in Electric Power Systems Research, volume 77, number 11, 2007.

[6] D. Dujic, "PLL part 2", Industrial electronics 1 course at EPFL, Lecture notes 12, slide 25, 2016.

[7] Arcteq Relays Ltd. Finland, "Application Note – New solution to feeder earth-fault protection," August 2017. [Online]. Available: https://arcteq.fi/wp-content/uploads/2017/08/Application-Note-AQ-200-new-solution-to-feeder-earth-fault-protection.pdf. [Accessed 5 March 2019].

[8] T. M. C. Le, "Couplage onduleurs photovoltaïques et réseau, aspects contrôle / commande et rejet de perturbations," Université de Grenoble, Grenoble, 2012.

[9] Joint Working Group B5/C6.26/CIRED, "Protection of Distribution Systems with Distributed Energy Resources", Chapters 1-4, Final Report, September 19, 2014.

[10] ABB Group, Line Distance Protection REL650. Technical Manual, Västerås: ABB, 2011.

[11] P. Romano, M. Pignati and M. Paolone, "Integration of an IEEE Std. C37.118 compliant PMU into a real-time simulator," *2015 IEEE Eindhoven PowerTech*, Eindhoven, Netherlands, 2015, pp. 1-6, doi: 10.1109/PTC.2015.7232794.

9 Appendices

Appendix 1. *PowerFactory* model provided by SIG

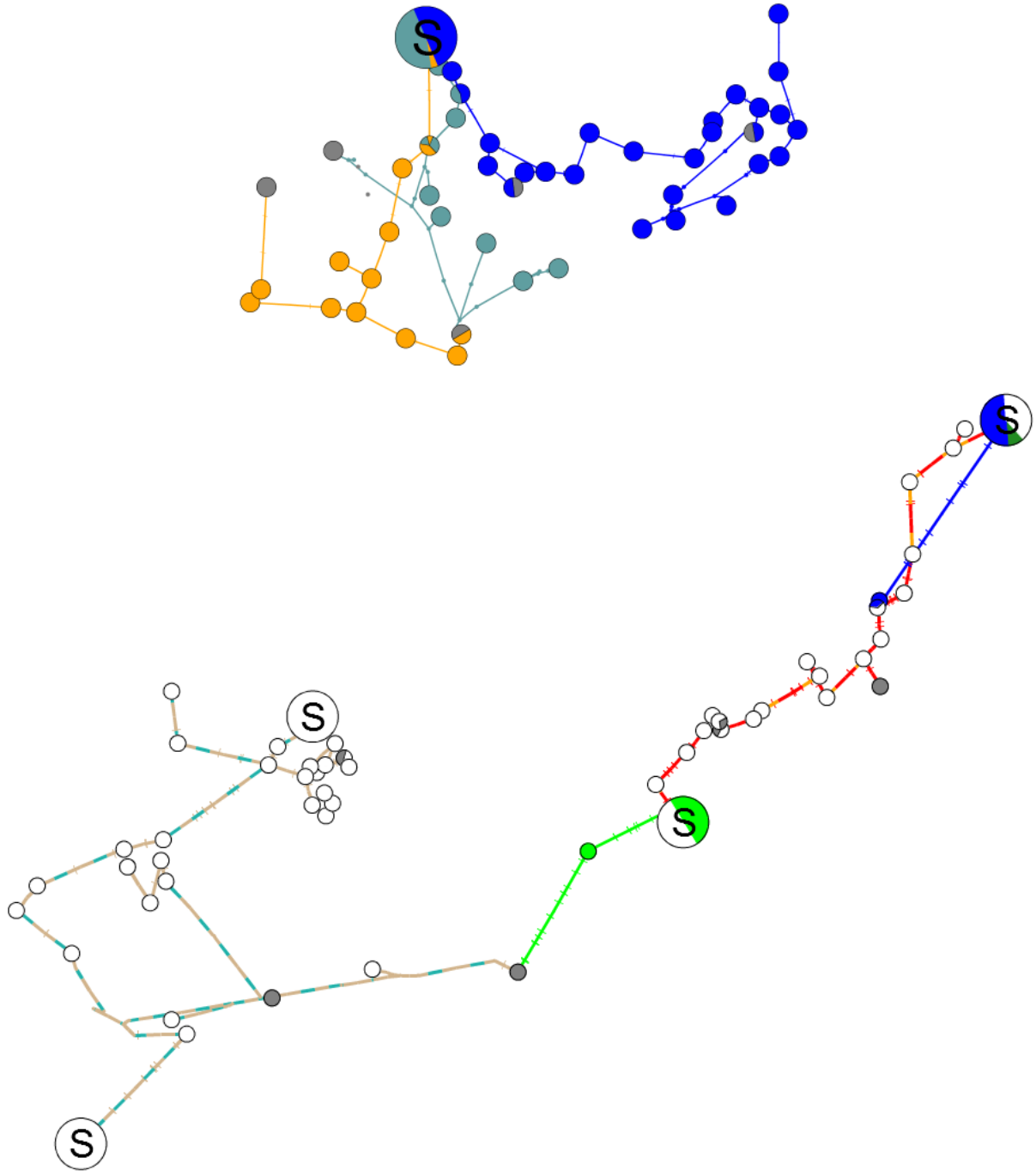

Appendix 2. EMTP-RV models of the other portions of the grid

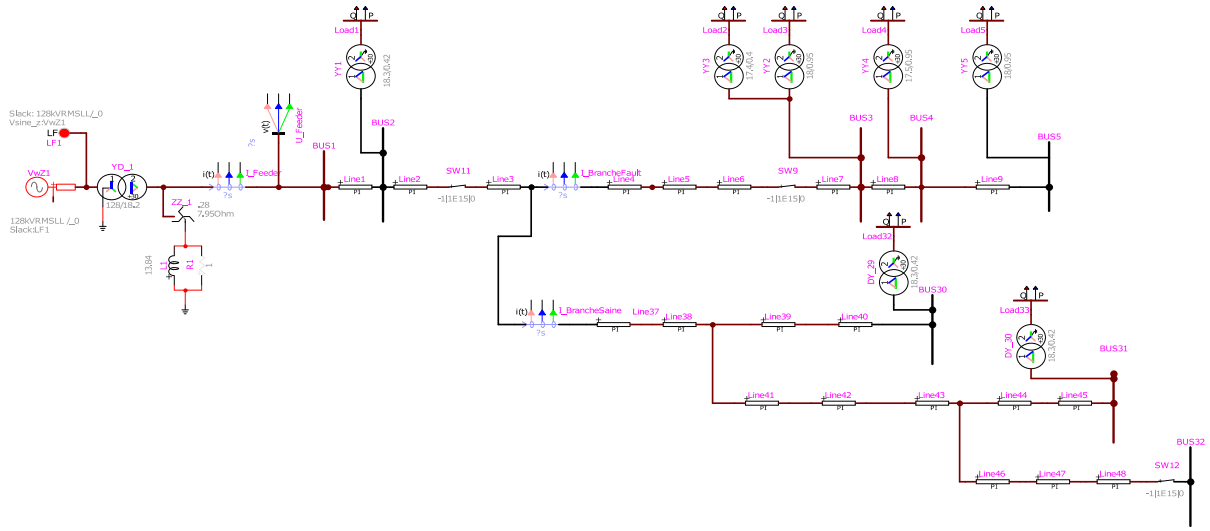

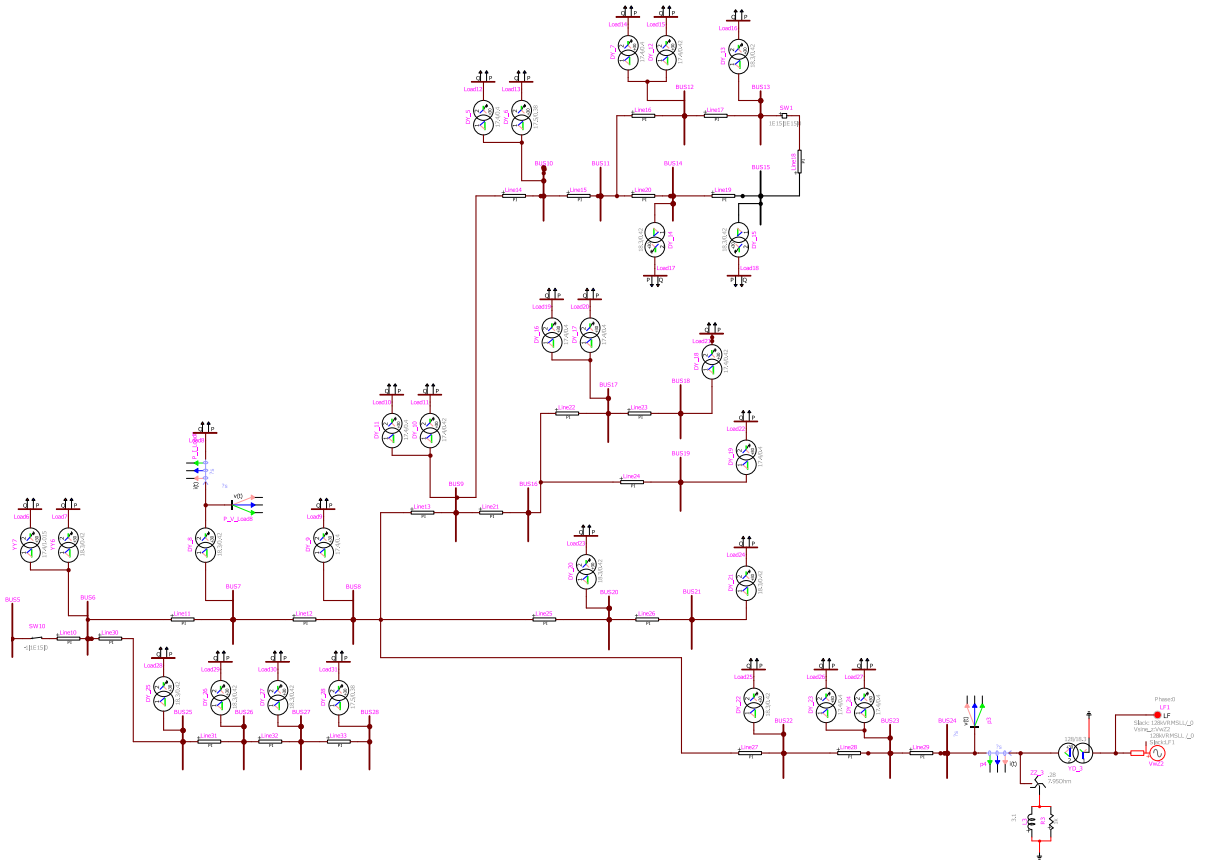

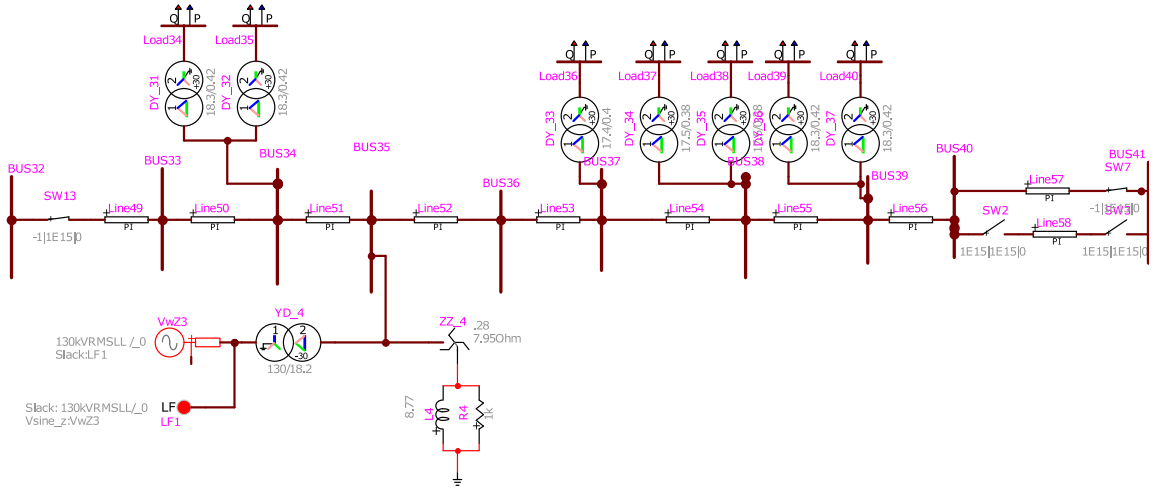
Load34
Load35
DY_31
DY_32
18,3|0,42
BUS32
BUS33
BUS34
BUS35
BUS36
BUS37
BUS38
BUS39
BUS40
BUS41
SW13
SW2
SW7
Line49
Line50
Line51
Line52
Line53
Line54
Line55
Line56
Line57
Line58
PI
-1|1E15|0
1E15|1E15|0
Load36
Load37
Load38
Load39
Load40
DY_33
DY_34
DY_35
DY_37
17,4|0,4
17,5|0,38
VwZ3
YD_4
ZZ_4
130kVRMSLL /_0
Slack:LF1
130/18.2
,28
7,95Ohm
Slack: 130kVRMSLL/_0
Vsine_z:VwZ3
LF
LF1
8,77
L4
R4
1K

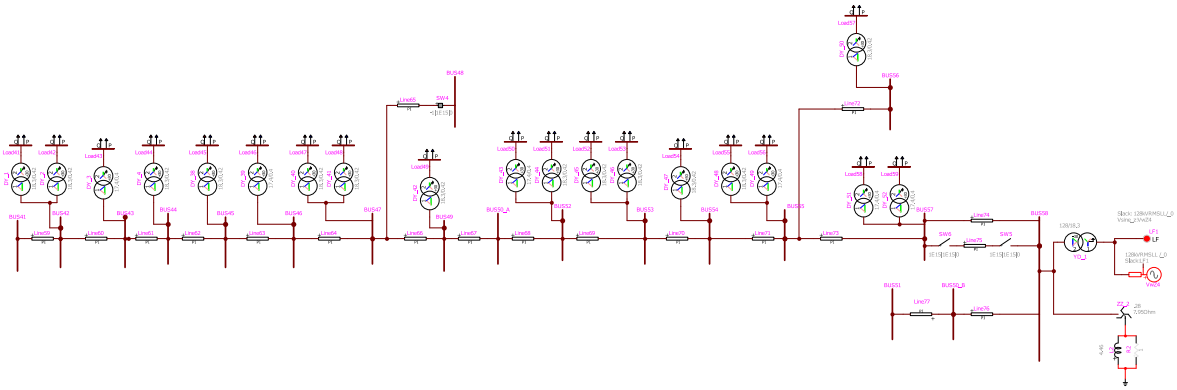

Appendix 3. Parametric analysis of symmetrical faults

a. Cases 1 to 4: PV at BUS5, SC at BUS32

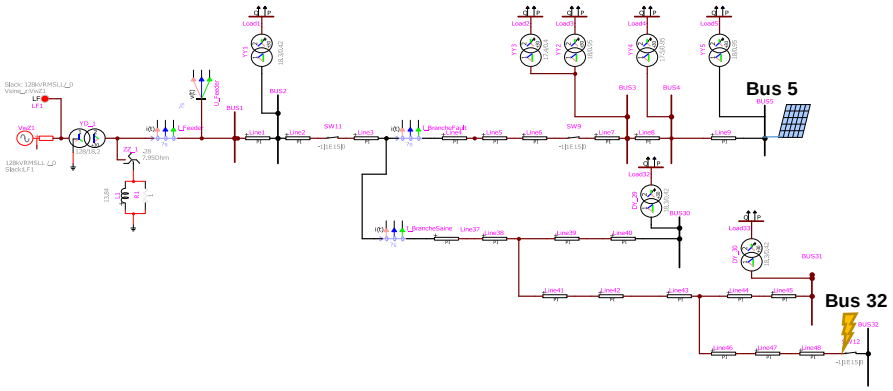

b. Cases 5 and 6: PV at BUS2 and SC at BUS32

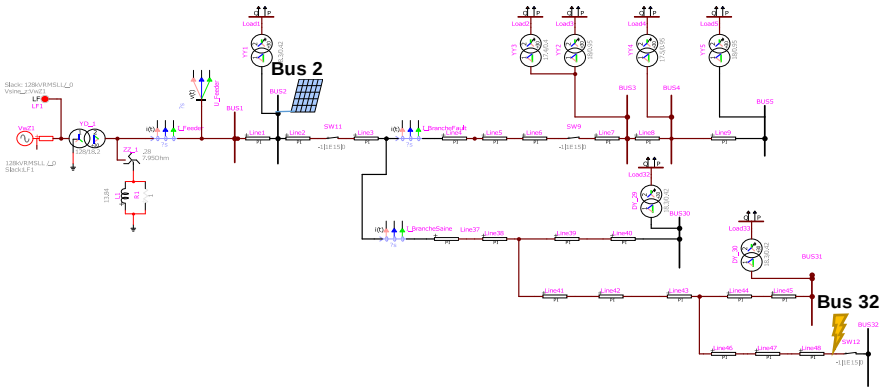

c. Cases 7 to 9: PV at BUS32 and SC BUS32

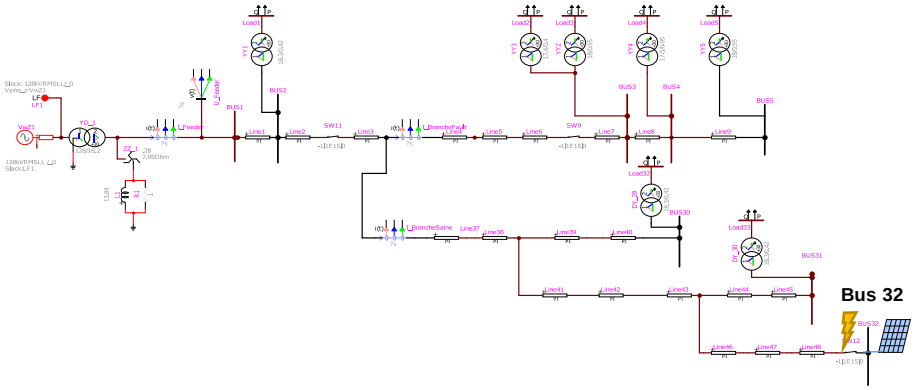

d. Cases 10 to 13: PV at BUS32 and SC at BUS5

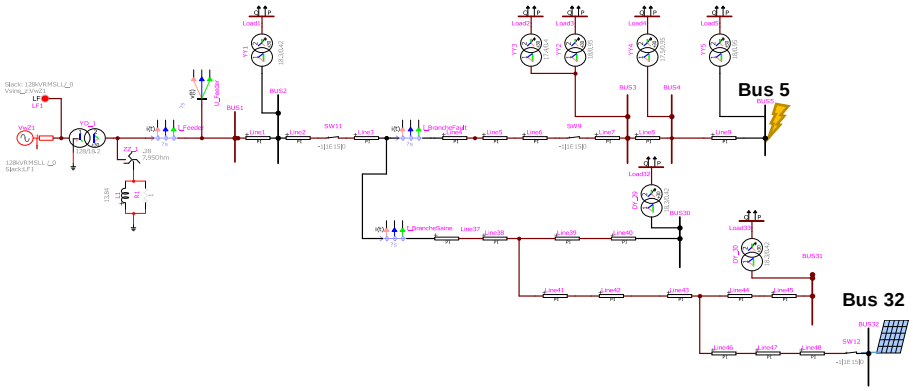

e. Cases 14 to 16: PV at BUS2 and SC at BUS5

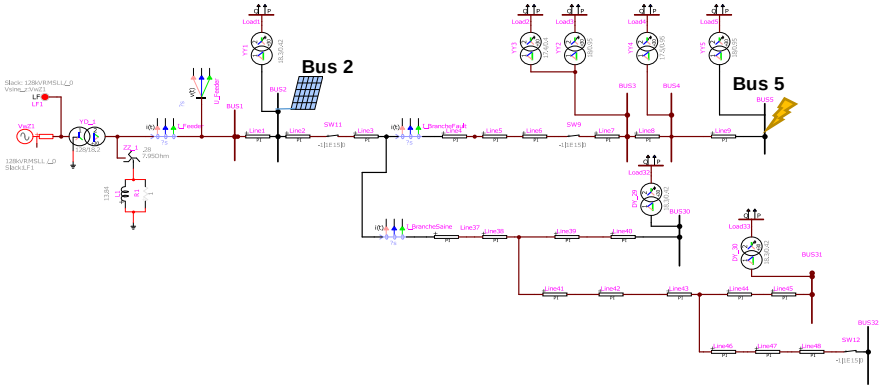

f. Case 17 to 19: PV at BUS5 and SC at BUS5

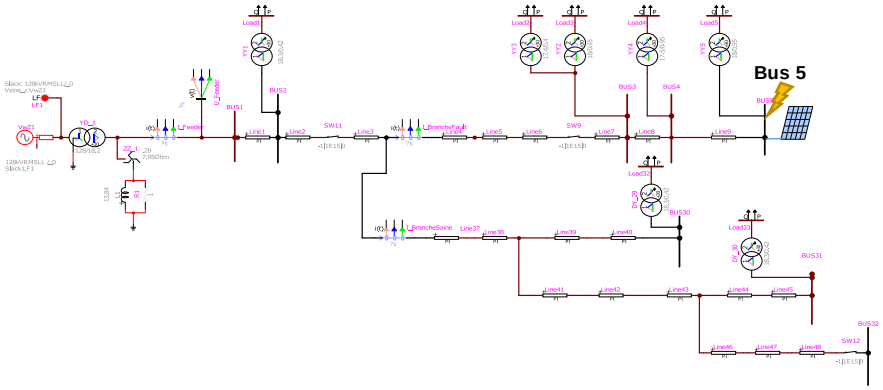

g. Case 20 to 24: PV at BUS32 and SC at BUS2

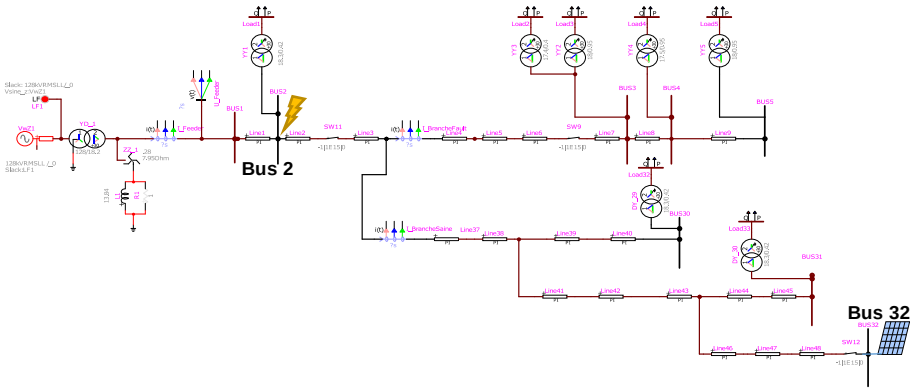

h. Results of the parametric analysis

Case N°	Change between cases	BUS32	BUS5	BUS2	ABCg, Rg=0		RMS Current [A]				Note
		PV [MW]	PV [MW]	PV [MW]	Fault R [Ω]	Fault Loc	I_Feeder	I_Fault	I_FaultedLine	I_PV	
1	Fault on BUS32 with 0 PV	0	0	0	8	BUS32	1098	1057	1061	0	
2	2 MW PV added to BUS5	0	2	0	8	BUS32	1041	1063	1067	162	
3	4 MW PV added to BUS5	0	6	0	8	BUS32	927	1075	1079	386	Blinding
4	2 MW PV substracted from BUS5	0	4	0	8	BUS32	984	1069	1073	282	
5	Moving PV to BUS2	0	0	2	8	BUS32	1040	1062	1066	156	
6	2 MW added to BUS2	0	0	4	8	BUS32	982	1067	1071	286	Blinding
7	Moving PV to BUS32	2	0	0	8	BUS32	1050	1074	1012	247	
8	2 MW PV added to BUS 32	4	0	0	8	BUS32	1001	1091	963	417	
9	2 MW PV added to BUS 32	6	0	0	8	BUS32	953	1017	915	551	Blinding
10	Moving fault to BUS 5 with 0 PV	0	0	0	8	BUS5	1162	1122	1155	0	
11	2 MW PV added to BUS32	2	0	0	8	BUS5	1104	1128	1162	161	
12	2 MW PV added to BUS32	4	0	0	8	BUS5	1045	1135	1169	276	
13	2 MW PV added to BUS32	6	0	0	8	BUS5	987	1140	1175	365	Blinding
14	Moving PV to BUS2	0	0	2	8	BUS5	1102	1127	1161	161	
15	2 MW PV added to BUS2	0	0	4	8	BUS5	1043	1132	1166	294	
16	2 MW PV added to BUS2	0	0	6	8	BUS5	984	1137	1172	402	Blinding
17	Moving PV to BUS5	0	2	0	8	BUS5	1108	1133	1102	203	
18	2 MW PV added to BUS5	0	4	0	8	BUS5	1054	1145	1048	351	
19	2 MW PV added to BUS5	0	8	0	8	BUS5	948	1167	941	584	Blinding
20	Moving fault to BUS2 with 0 PV	0	0	0	8	BUS2	1253	1211	NA	0	
21	2 MW PV added to BUS32	2	0	0	8	BUS2	1194	1217	NA	154	
22	2 MW PV added to BUS32	4	0	0	8	BUS2	1135	1222	NA	264	
23	2 MW PV added to BUS32	8	0	0	8	BUS2	1017	1233	NA	428	
24	2 MW PV added to BUS32	10	0	0	8	BUS2	959	1237	NA	519	Blinding